

1 SEARCH FOR PRODUCTION OF A HIGGS BOSON AND A SINGLE TOP
2 QUARK IN MULTILEPTON FINAL STATES IN pp COLLISIONS AT $\sqrt{s} = 13$
3 TeV.

4 by

5 Jose Andres Monroy MontaÑez

6 A DISSERTATION

7 Presented to the Faculty of

8 The Graduate College at the University of Nebraska

In Partial Fulfilment of Requirements

10 For the Degree of Doctor of Philosophy

11 Major: Physics and Astronomy

12 Under the Supervision of Kenneth Bloom and Aaron Dominguez

13 Lincoln, Nebraska

14 July, 2018

15 SEARCH FOR PRODUCTION OF A HIGGS BOSON AND A SINGLE TOP
16 QUARK IN MULTILEPTON FINAL STATES IN pp COLLISIONS AT $\sqrt{s} = 13$
17 TeV.

18 Jose Andres Monroy Montañez, Ph.D.

19 University of Nebraska, 2018

20 Adviser: Kenneth Bloom and Aaron Dominguez

²¹ Table of Contents

| | |
|--|-------------|
| ²² Table of Contents | iii |
| ²³ List of Figures | vi |
| ²⁴ List of Tables | viii |
| ²⁵ 1 INTRODUCTION | 1 |
| ²⁶ 2 Theoretical approach | 2 |
| ²⁷ 2.1 Introduction | 2 |
| ²⁸ 2.2 Standard model of particle physics | 3 |
| ²⁹ 2.2.1 Fermions | 5 |
| ³⁰ 2.2.1.1 Leptons | 6 |
| ³¹ 2.2.1.2 Quarks | 8 |
| ³² 2.2.2 Fundamental interactions | 12 |
| ³³ 2.2.3 Gauge Bosons | 18 |
| ³⁴ 2.3 Electroweak unification and the Higgs mechanism | 19 |
| ³⁵ 2.3.1 Spontaneous symmetry breaking | 27 |
| ³⁶ 2.3.2 Higgs mechanism | 31 |
| ³⁷ 2.3.3 Masses of the gauge bosons | 33 |

| | | | |
|----|----------|---|-----------|
| 38 | 2.3.4 | Masses of the fermions | 34 |
| 39 | 2.3.5 | The Higgs field | 35 |
| 40 | 2.3.6 | Higgs boson production mechanisms at LHC. | 37 |
| 41 | 2.3.7 | Higgs decay channels | 40 |
| 42 | 2.4 | Associated Production of Higgs Boson and Single Top Quark. | 41 |
| 43 | 2.5 | The CP-mixing in tH processes | 46 |
| 44 | 3 | The CMS experiment at the LHC | 51 |
| 45 | 3.1 | Introduction | 51 |
| 46 | 3.2 | The LHC | 52 |
| 47 | 3.3 | The CMS experiment | 56 |
| 48 | 4 | Search for production of a Higgs boson and a single top quark in multilepton final states in pp collisions at $\sqrt{s} = 13$ TeV | 58 |
| 50 | 4.1 | Introduction | 58 |
| 51 | 4.2 | Data and MC Samples | 60 |
| 52 | 4.2.1 | Full 2016 dataset and MC samples | 60 |
| 53 | 4.2.2 | Triggers | 63 |
| 54 | 4.2.2.1 | Trigger efficiency scale factors | 63 |
| 55 | 4.3 | Object Identification and event selection | 64 |
| 56 | 4.3.1 | Jets and b tagging | 64 |
| 57 | 4.3.2 | Lepton selection | 65 |
| 58 | 4.3.3 | Lepton selection efficiency | 66 |
| 59 | 4.4 | Background predictions | 67 |
| 60 | 4.5 | Signal discrimination | 68 |
| 61 | 4.5.1 | Classifiers response | 72 |
| 62 | 4.6 | Additional discriminating variables | 75 |

| | | |
|----|---|-----------|
| 63 | 5 The CMS forward pixel detector | 78 |
| 64 | 5.0.1 The phase 1 FPix upgrade | 78 |
| 65 | 5.0.2 FPix module production line | 78 |
| 66 | 5.0.3 The Gluing stage | 78 |
| 67 | 5.0.4 The Encapsulation stage | 78 |
| 68 | 5.0.5 The FPix module production yields | 78 |
| 69 | Bibliography | 78 |
| 70 | References | 79 |

⁷¹ List of Figures

| | | | |
|----|------|--|----|
| 72 | 1.1 | ^{14}N neutron capture in a PECVD polymerized pyridine film. The Q-value of this reaction is 626 keV. Taken from [22] | 1 |
| 74 | 2.1 | Standard model of particle physics. | 4 |
| 75 | 2.2 | WI transformations between quarks | 11 |
| 76 | 2.3 | Fundamental interactions in nature. | 12 |
| 77 | 2.4 | SM interactions diagrams | 14 |
| 78 | 2.5 | Neutral current processes | 20 |
| 79 | 2.6 | Spontaneous symmetry breaking mechanism | 28 |
| 80 | 2.7 | SSB Potential form | 29 |
| 81 | 2.8 | Potential for complex scalar field | 30 |
| 82 | 2.9 | SSB mechanism for complex scalar field | 31 |
| 83 | 2.10 | Proton-Proton collision | 37 |
| 84 | 2.11 | Higgs production mechanism Feynman diagrams | 38 |
| 85 | 2.12 | Higgs production cross section and decay branching ratios | 39 |
| 86 | 2.13 | Associated Higgs production mechanism Feynman diagrams | 42 |
| 87 | 2.14 | Cross section for tHq process as a function of C_t | 45 |
| 88 | 2.15 | Cross section for tHW process as a function of κ_{Htt} | 45 |
| 89 | 2.16 | NLO cross section for tX_0 and $t\bar{t}X_0$ | 48 |

| | | |
|-----|--|----|
| 90 | 2.17 NLO cross section for tWX_0 , $t\bar{t}X_0$ and $tWX_0 + t\bar{t}X_0 + \text{interference}$. . . | 50 |
| 91 | 3.1 ref. C.Lefevre, “The CERN accelerator complex,” (2008). CERN-DI- | |
| 92 | 0812015. | 53 |
| 93 | 3.2 ref. J.-L. Caron , “Layout of the LEP tunnel including future LHC in- | |
| 94 | frastructures.. L’ensemble du tunnel LEP avec les futures infrastructures | |
| 95 | LHC.”, https://cds.cern.ch/record/841542 (Nov, 1993). AC Collection. | |
| 96 | Legacy of AC. Pictures from 1992 to 2002.. | 54 |
| 97 | 3.3 ref. ACTeam, “Diagram of an LHC dipole magnet. Schéma d’un aimant | |
| 98 | dipôle du LHC,” (1999). CERN-DI-9906025. | 55 |
| 99 | 3.4 ref: CMS Collaboration, “Detector Drawings”, CMS-PHO-GEN-2012-002, | |
| 100 | http://cds.cern.ch/record/1433717 , 2012. | 57 |
| 101 | 4.1 The two leading-order diagrams of tHq production. | 59 |
| 102 | 4.2 Input variables to the BDT for signal discrimination normalized. | 69 |
| 103 | 4.3 Input variables to the BDT for signal discrimination not normalized. . . | 71 |
| 104 | 4.4 BDT inputs as seen by TMVA against $t\bar{t}$ | 72 |
| 105 | 4.5 BDT inputs as seen by TMVA against $t\bar{t}V$ | 73 |
| 106 | 4.6 Correlation matrices for the input variables in the TMVA. | 74 |
| 107 | 4.7 MVA classifiers performance. | 74 |
| 108 | 4.8 Additional discriminating variables distributions. | 76 |

¹⁰⁹ List of Tables

| | | | |
|-----|------|--|----|
| 110 | 2.1 | Fermions of the SM. | 6 |
| 111 | 2.2 | Leptons properties. | 8 |
| 112 | 2.3 | Quarks properties. | 9 |
| 113 | 2.4 | Fermion weak isospin and weak hypercharge multiplets. | 10 |
| 114 | 2.5 | Fundamental interactions features. | 15 |
| 115 | 2.6 | SM gauge bosons. | 19 |
| 116 | 2.7 | Higgs boson properties. | 36 |
| 117 | 2.8 | Predicted branching ratios for a SM Higgs boson with $m_H = 125 \text{ GeV}/c^2$ | 41 |
| 118 | 2.9 | Predicted SM cross sections for tH production at $\sqrt{s} = 13 \text{ TeV}$ | 43 |
| 119 | 2.10 | Predicted enhancement of the tHq and tHW cross sections at LHC | 46 |
| 120 | 4.1 | Signal samples and their cross section and branching fraction. | 60 |
| 121 | 4.2 | κ_V and κ_t combinations. | 61 |
| 122 | 4.3 | List of background samples used in this analysis (CMSSW 80X). | 62 |
| 123 | 4.4 | Leading-order $t\bar{t}W$ and $t\bar{t}Z$ samples used in the signal BDT training. | 62 |
| 124 | 4.5 | Table of high-level triggers that we consider in the analysis. | 63 |
| 125 | 4.6 | Trigger efficiency scale factors and associated uncertainties. | 64 |
| 126 | 4.7 | Requirements on each of the three muon selections. | 65 |
| 127 | 4.8 | Criteria for each of the three electron selections. | 66 |

| | | |
|-----|--|----|
| 128 | 4.9 MVA input discriminating variables | 70 |
| 129 | 4.10 TMVA input variables ranking for BDTA_GRAD method | 75 |
| 130 | 4.11 TMVA configuration used in the BDT training. | 75 |
| 131 | 4.12 ROC-integral for all the testing cases. | 77 |

¹³² Chapter 1

¹³³ INTRODUCTION

Figure 1.1: ^{14}N neutron capture in a PECVD polymerized pyridine film. The Q-value of this reaction is 626 keV. Taken from [22]

¹³⁴ **Chapter 2**

¹³⁵ **Theoretical approach**

¹³⁶ **2.1 Introduction**

¹³⁷ The physical description of the universe is a challenge that physicists have faced by
¹³⁸ making theories that refine existing principles and proposing new ones in an attempt
¹³⁹ to embrace emerging facts and phenomena.

¹⁴⁰ At the end of 1940s Julian Schwinger [11] and Richard P. Feynman [12], based in
¹⁴¹ the work of Sin-Itiro Tomonaga [13], developed an electromagnetic theory consistent
¹⁴² with special relativity and quantum mechanics that describes how matter and light
¹⁴³ interact; the so-called “quantum eletrodynamics” (QED) had born.

¹⁴⁴

¹⁴⁵ QED has become the guide in the development of theories that describe the universe.
¹⁴⁶ It was the first example of a quantum field theory (QFT), which is the theoretical
¹⁴⁷ framework for building quantum mechanical models that describes particles and their
¹⁴⁸ interactions. QFT is composed of a set of mathematical tools that combines classical
¹⁴⁹ fields, special relativity, and quantum mechanics while keeping the quantum point
¹⁵⁰ particles and locality ideas.

151 This chapter gives an overview of the standard model of particle physics, starting
 152 with a description of the particles and interactions that compose it, followed by a
 153 description of the electroweak interaction, the Higgs boson and the associated pro-
 154 duction of Higgs boson and a single top quark (tH). The description contained in
 155 this chapter is based on references [1–3].

156 2.2 Standard model of particle physics

157 Particle physics at the fundamental level is modeled in terms of a collection of in-
 158 teracting particles and fields in a theory known as the “standard model of particle
 159 physics (SM)”¹.

160 The full picture of the SM is composed of three fields², whose excitations are inter-
 161 preted as particles called mediators or force-carriers; a set of fields, whose excitations
 162 are interpreted as elementary particles, interacting through the exchange of those
 163 mediators and a field that give the mass to elementary particles. Figure 2.1 shows an
 164 scheme of the SM particles organization. In addition to the particles in the scheme
 165 (but not listed in it), their corresponding anti-particles, with opposite quantum num-
 166 bers, are also part of the picture; some particles are their own anti-particles, like
 167 photon or Higgs, or anti-particle is already listed like in the W^+ and W^- case.

168

169 The mathematical formulation of the SM is based on group theory and the use of
 170 Noether’s theorem [17] which states that for a physical system modeled by a La-
 171 grangian that is invariant under a group of transformations a conservation law is

¹ The formal and complete treatment of the SM is out of the scope of this document, however a plenty of textbooks describing it at several levels are available in the literature. The treatment in “An Introduction To Quantum Field Theory (Frontiers in Physics)” by Michael E. Peskin and Dan V. Schroeder is quite comprehensive and detailed.

² Note that gravitational field is not included in the standard model formulation

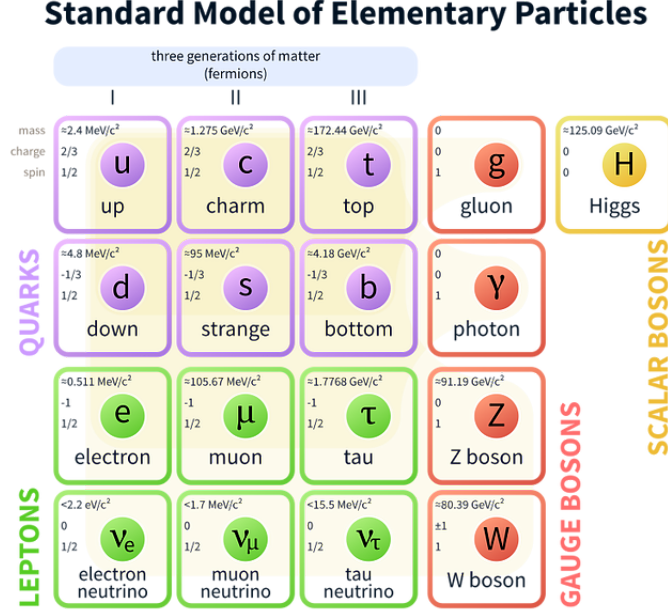


Figure 2.1: Schematic representation of the Standard model of particle physics. SM is a theoretical model intended to describe three of the four fundamental forces of the universe in terms of a set of particles and their interactions. [18].

172 expected. For instance, a system described by a time-independent Lagrangian is
 173 invariant (symmetric) under time changes (transformations) with the total energy
 174 conservation law as the expected conservation law. In QED, the charge operator
 175 (Q) is the generator of the $U(1)$ symmetry which according to the Noether's theorem
 176 means that there is a conserved quantity; this conserved quantity is the electric charge
 177 and thus the law conservation of electric charge is established.

178

179 In the SM, the symmetry group $SU(3)_C \otimes SU(2)_L \otimes U(1)_Y$ describes three of the
 180 four fundamental interactions in nature(see section 2.2.2): strong interaction(SI),
 181 weak interaction(WI) and electromagnetic interactions (EI) in terms of symmetries
 182 associated to physical quantities:

- 183 • Strong: $SU(3)_C$ associated to color charge

- 184 • Weak: $SU(2)_L$ associated to weak isospin and chirality
 185 • Electromagnetic: $U(1)_Y$ associated to weak hypercharge and electric charge

186 It will be shown that the electromagnetic and weak interactions are combined in
 187 the so-called electroweak interaction where chirality, hypercharge, weak isospin and
 188 electric charge are the central concepts.

189 **2.2.1 Fermions**

190 The basic constituents of the ordinary matter at the lowest level, which form the set
 191 of elementary particles in the SM formulation, are quarks and leptons. All of them
 192 have spin 1/2, therefore they are classified as fermions since they obey Fermi-Dirac
 193 statistics. There are six “flavors” of quarks and three of leptons organized in three
 194 generations, or families, as shown in table 2.1.

195
 196 There is a mass hierarchy between generations where the higher generation particles
 197 decays to the lower one which can explain why the ordinary matter is made of particles
 198 in the first generation. In the SM, neutrinos are modeled as massless particles so they
 199 are not subject to this mass hierarchy; however, today it is known that neutrinos are
 200 massive so the hierarchy could be restated. The reason behind this mass hierarchy is
 201 one of the most important open questions in particle physics, and it becomes more
 202 puzzling when noticing that the mass difference between first and second generation
 203 fermions is small compared to the mass difference with respect to the third generation.
 204 Usually, the second and third generation fermions are produced in high energy pro-
 205 cesses, like the ones recreated in the particle accelerators.

| | | Generation | | |
|---------|----------------------|-------------------------------|-----------------------------|-----------------------------|
| Type | | 1st | 2nd | 3rd |
| Leptons | Charged | Electron (e) | Moun(μ) | Tau (τ) |
| | Neutral | Electron neutrino (ν_e) | Muon neutrino (ν_μ) | Tau neutrino (ν_τ) |
| Quarks | Up-type Down-type | Up (u) Down (d) | Charm (c) Starnge (s) | Top (t) Bottom (b) |

Table 2.1: Fermions of the SM. Quarks and leptons comes in six flavors each and are organized in three generations or families composed of two pairs of closely related particles. The close relationship is motivated by the fact that WI between leptons is limited to the members of the same generation. Generations differs by mass in a way that have been interpreted as a masss hierarchy.

207 2.2.1.1 Leptons

208 A lepton is an elementary particle that is not subject to the SI. As seen in table 2.1,
 209 there are two types of leptons, the charged ones (electron, muon and tau) and the
 210 neutral ones (the three neutrinos). The electric charge (Q) is the property that gives
 211 leptons the ability to participate in the EI. From the classical point of view, Q plays
 212 a central role determining, among others, the strength of the electric field through
 213 which the electromagnetic force is exerted. It is clear that neutrinos are not affected
 214 by EI because they don't carry electric charge.

215

216 Another feature of the leptons that is fundamental in the mathematical description
 217 of the SM is the chirality, which is closely related to spin and helicity. Helicity de-
 218 fine the handedness of a particle by relating its spin and momentum such that if
 219 they are parallel then the particle is right-handed; if spin and momentum are an-
 220 tiparallel the particle is said to be left-handed. The study of parity conservation
 221 (or violation) in β -decay have shown that only left-handed electrons/neutrinos or
 222 right-handed positrons/anti-neutrinos are created [19]; the inclusion of that feature
 223 in the theory was reached by using projection operators for helicity, however, helicity
 224 is frame dependent for massive particles which makes it not Lorentz invariant and

225 then another related attribute has to be used: *chirality*.

226

227 Chirality is a purely quantum attribute which makes it not so easy to describe in
 228 graphical terms but it defines how the wave function of a particle transforms under
 229 certain rotations. As with helicity, there are two chiral states, left-handed chiral
 230 (L) and right-handed chiral (R). In the highly relativistic limit where $E \approx p \gg m$
 231 helicity and chirality converge, becoming exactly the same for massless particles. In
 232 the following when referring to left-handed (right-handed) it means left-handed chiral
 233 (right-handed chiral). The fundamental fact about chirality is that while EI and SI
 234 are not sensitive to chirality, in WI left-handed and right-handed fermions are treated
 235 asymmetrically, such that only left handed fermions and right-handed anti-fermions
 236 are allowed to couple to WI mediators, which is a violation of parity. The way to
 237 translate this statement in a formal mathematical formulation is based on the isospin
 238 symmetry group $SU(2)_L$.

239 Each generation of leptons is seen as a weak isospin doublet.³ The left-handed charged
 240 lepton and its associated left-handed neutrino are arranged in doublets of weak isospin
 241 $T=1/2$ while their right-handed partners are singlets:

$$\begin{pmatrix} \nu_l \\ l \end{pmatrix}_L, l_R := \begin{pmatrix} \nu_e \\ e \end{pmatrix}_L, \begin{pmatrix} \nu_\mu \\ \mu \end{pmatrix}_L, \begin{pmatrix} \nu_\tau \\ \tau \end{pmatrix}_L, e_R, \mu_R, \tau_R, \nu_{eR}, \nu_{\mu R}, \nu_{\tau R} \quad (2.1)$$

242 The isospin third component refers to the eigenvalues of the weak isospin operator
 243 which for doublets is $T_3 = \pm 1/2$, while for singlets it is $T_3 = 0$. The physical meaning
 244 of this doublet-singlet arrangement falls in that the WI couples the two particles in
 245 the doublet by exchanging the interaction mediator while the singlet member is not
 246 involved in WI. The main properties of the leptons are summarized in table 2.2.

³ The weak isospin is an analogy of the isospin symmetry in strong interaction where neutron and proton are affected equally by strong force but differ in their charge.

247

248 Altough all three flavor neutrinos have been observed, their masses remain unknown
 249 and only some estimations have been made [20]. The main reason is that the fla-
 250 vor eigenstates are not the same as the mass eigenstates which imply that when a
 251 neutrino is created its mass state is a linear combination of the three mass eigen-
 252 states and experiments can only probe the squared difference of the masses. The
 253 Pontecorvo-Maki-Nakagawa-Sakata (PMNS) mixing matrix encode the relationship
 254 between flavor and mass eigenstates.

| Lepton | Q(e) | T_3 | L_e | L_μ | L_τ | Mass (MeV/c ²) | Lifetime (s) |
|------------------------------|------|-------|-------|---------|----------|----------------------------|--------------------------------|
| Electron (e) | -1 | -1/2 | 1 | 0 | 0 | 0.5109989461(31) | Stable |
| Electron neutrino(ν_e) | 0 | 1/2 | 1 | 0 | 0 | Unknown | Unknown |
| Muon (μ) | -1 | -1/2 | 0 | 1 | 0 | 105.6583745(24) | $2.1969811(22) \times 10^{-6}$ |
| Muon neutrino (ν_μ) | 0 | 1/2 | 0 | 1 | 0 | Unknown | Unknown |
| Tau (τ) | -1 | -1/2 | 0 | 0 | 1 | 1776.86(12) | $290.3(5) \times 10^{-15}$ |
| Tau neutrino (τ_μ) | 0 | 1/2 | 0 | 0 | 1 | Unknown | Unknown |

Table 2.2: Leptons properties [21]. Q: electric charge, T_3 : weak isospin. Only left-handed leptons and right-handed anti-leptons participate in the WI. Anti-particles with inverted T_3 , Q and lepton number complete the leptons set but are not listed. Right-handed leptons and left-handed anti-leptons, neither listed, form weak isospin singlets with $T_3 = 0$ and do not take part in the weak interaction.

255

256 2.2.1.2 Quarks

257 Quarks are the basic constituents of protons, neutrons and other non-elementary
 258 particles. The way quarks join to form bound states, called “hadrons”, is through the
 259 SI. Quarks are affected by all the fundamental interactions which means that they
 260 carry all the four types of charges: color, electric charge, weak isospin and mass.

261

| Flavor | Q(e) | I_3 | T_3 | B | C | S | T | B' | Y | Color | Mass (MeV/c ²) |
|------------|------|-------|-------|-----|---|----|---|------|------|-------|------------------------------------|
| Up (u) | 2/3 | 1/2 | 1/2 | 1/3 | 0 | 0 | 0 | 0 | 1/3 | r,b,g | $2.2^{+0.6}_{-0.4}$ |
| Charm (c) | 2/3 | 0 | 1/2 | 1/3 | 1 | 0 | 0 | 0 | 4/3 | r,b,g | $1.28 \pm 0.03 \times 10^3$ |
| Top(t) | 2/3 | 0 | 1/2 | 1/3 | 0 | 0 | 1 | 0 | 4/3 | r,b,g | $173.1 \pm 0.6 \times 10^3$ |
| Down(d) | -1/3 | -1/2 | -1/2 | 1/3 | 0 | 0 | 0 | 0 | 1/3 | r,b,g | $4.7^{+0.5}_{-0.4}$ |
| Strange(s) | -1/3 | 0 | -1/2 | 1/3 | 0 | -1 | 0 | 0 | -2/3 | r,b,g | 96^{+8}_{-4} |
| Bottom(b) | -1/3 | 0 | -1/2 | 1/3 | 0 | 0 | 0 | -1 | -2/3 | r,b,g | $4.18^{+0.04}_{-0.03} \times 10^3$ |

Table 2.3: Quarks properties [21]. Q: electric charge, I_3 : isospin, T_3 : weak isospin, B: baryon number, C: charmness, S: strangeness, T: topness, B' : bottomness, Y: hypercharge. Anti-quarks posses the same mass and spin as quarks but all charges (color, flavor numbers) have opposite sign.

262 Table 2.3 summarizes the features of quarks, among which the most particular is
 263 their fractional electric charge. Note that fractional charge is not a problem, given
 264 that quarks are not found isolated, but serves to explain how composed particles are
 265 formed out of two or more valence quarks⁴.

266

267 Color charge is the responsible for the SI between quarks and is the symmetry
 268 ($SU(3)_C$) that defines the formalism to describe SI. There are three colors: red (r),
 269 blue(b) and green(g) and their corresponding three anti-colors; thus each quark carries
 270 one color unit while anti-quarks carries one anti-color unit. As said above, quarks are
 271 not allowed to be isolated due to the color confinement effect, therefore their features
 272 have been studied indirectly by observing their bound states created when:

- 273 • one quark with a color charge is attracted by an anti-quark with the correspond-
 274 ing anti-color charge forming a colorless particle called a “meson.”
- 275 • three quarks (anti-quarks) with different color (anti-color) charges are attracted
 276 among them forming a colorless particle called a “baryon(anti-baryon).”

⁴ Hadrons can contain an indefinite number of virtual quarks and gluons, known as the quark and gluon sea, but only the valence quarks determine hadrons’ quantum numbers.

277 In the first version of the quark model (1964), M. Gell-Mann [22] and G. Zweig [23,24]
 278 developed a consistent way to classify hadrons according to their properties. Only
 279 three quarks (u, d, s) were involved in a scheme in which all baryons have baryon
 280 number $B=1$ and therefore quarks have $B=1/3$; non-baryons have $B=0$. The scheme
 281 organize baryons in a two-dimensional space (I_3 - Y); Y (hypercharge) and I_3 (isospin)
 282 are quantum numbers related by the Gell-Mann-Nishijima formula [25,26]:

$$Q = I_3 + \frac{Y}{2} \quad (2.2)$$

283 where $Y = B + S + C + T + B'$ are the quantum numbers listed in table 2.3. Baryon
 284 number is conserved in SI and EI which means that single quarks cannot be created
 285 but in pairs $q - \bar{q}$.

286

287 Similar to leptons, there are six quark flavors organized in three generations (see table
 288 2.1) and follow a mass hierarchy which again implies that higher generations decay
 289 to first generation quarks.

| | Quarks | | | T_3 | Y_W | Leptons | | | T_3 | Y_W |
|----------|---|---|---|---|-------|--|--|--|---|-------|
| Doublets | $(\begin{smallmatrix} u \\ d' \end{smallmatrix})_L$ | $(\begin{smallmatrix} c \\ s' \end{smallmatrix})_L$ | $(\begin{smallmatrix} t \\ b' \end{smallmatrix})_L$ | $(\begin{smallmatrix} 1/2 \\ -1/2 \end{smallmatrix})$ | 1/3 | $(\begin{smallmatrix} \nu_e \\ e \end{smallmatrix})_L$ | $(\begin{smallmatrix} \nu_\mu \\ \mu \end{smallmatrix})_L$ | $(\begin{smallmatrix} \nu_\tau \\ \tau \end{smallmatrix})_L$ | $(\begin{smallmatrix} 1/2 \\ -1/2 \end{smallmatrix})$ | -1 |
| Singlets | u_R | c_R | t_R | 0 | 4/3 | ν_{eR} | $\nu_{\mu R}$ | $\nu_{\tau R}$ | 0 | -2 |

Table 2.4: Fermion weak isospin and weak hypercharge multiplets. Weak hypercharge is calculated through the Gell-Mann-Nishijima formula 2.2 but using the weak isospin and charge for quarks.

290

291 Isospin doublets of quarks are also defined (see table 2.4) and as for neutrinos, the
 292 mass eigenstates are not the same as the WI eigenstates which means that members of
 293 different quark generations are connected by the WI mediator; thus, up-type quarks

294 are coupled not to down-type quarks directly but to a superposition of down-type
 295 quarks (q'_d) via WI according to:

$$296 \quad q'_d = V_{CKM} q_d$$

$$\begin{pmatrix} d' \\ s' \\ b' \end{pmatrix} = \begin{pmatrix} V_{ud} & V_{us} & V_{ub} \\ V_{cd} & V_{cs} & V_{cb} \\ V_{td} & V_{ts} & V_{tb} \end{pmatrix} \begin{pmatrix} d \\ s \\ b \end{pmatrix} \quad (2.3)$$

297 where V_{CKM} is known as Cabibbo-Kobayashi-Maskawa (CKM) mixing matrix [27,28].

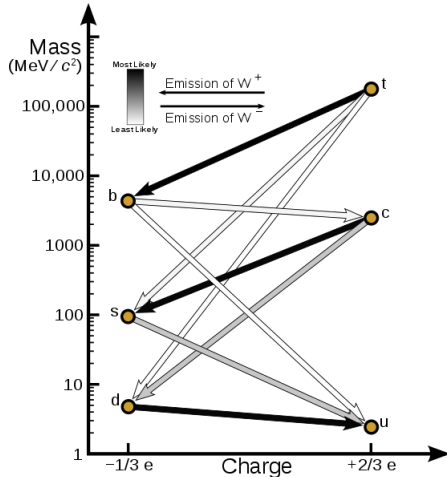


Figure 2.2: Transformations between quarks through WI. Higher generations quarks decay to first generation quarks by emitting a W boson. The arrow color indicates the likelihood of the transition according to the grey scale in the top left side which represent the CKM matrix parameters [29].

298 The weak decays of quarks are represented in the diagram of figure 2.2; again the
 299 CKM matrix plays a central role since it contains the probabilities for the different
 300 quark decay channels, in particular, note that quark decays are greatly favored be-
 301 tween generation members.

302

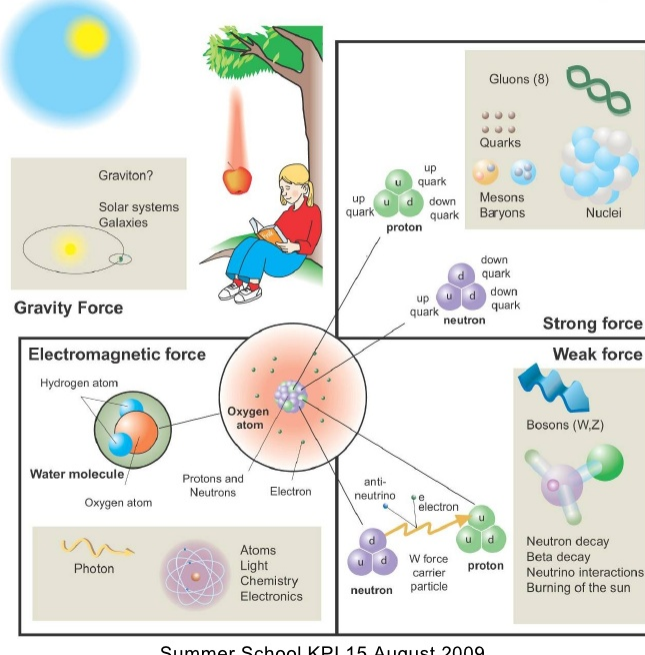
303 CKM matrix is a 3×3 unitary matrix parametrized by three mixing angles and the

304 *CP-mixing phase*; the latter is the parameter responsible for the CP-violation in the
 305 SM. The fact that the b quark decays almost all the times to a top quark is exploited
 306 in this thesis when making the selection of the signal events by requiring the presence
 307 of a jet tagged as a jet coming from a b quark in the final state. The effect of the
 308 *CP-mixing phase* on the cross section of associated production of Higgs boson and a
 309 single top process is also explored in this thesis.

310 2.2.2 Fundamental interactions

Fundamental interactions.

Illustration: Typoform



Summer School KPI 15 August 2009

Figure 2.3: Fundamental interactions in nature. Despite the many manifestations of forces in nature, we can track all of them back to one of the fundamental interactions. The most common forces are gravity and electromagnetic given that all of us are subject and experience them in everyday life.

311 Even though there are many manifestations of force in nature, like the ones repre-
 312 sented in figure 2.3, we can classify all of them into one of four fundamental interac-

313 tions:

- 314 ● *Electromagnetic interaction (EI)* affect particles that are “electrically charged,”
 315 like electrons and protons. It is described by QED combining quantum mechanics,
 316 special relativity and electromagnetism in order to explain how particles
 317 with electric charge interact through the exchange of photons, therefore, one
 318 says that “Electromagnetic Force” is mediated by “photons”. Figure 2.4a. shows
 319 a graphical representation, known as “feynman diagram”, of electron-electron
 320 scattering.
- 321 ● *Strong interaction (SI)* described by Quantum Chromodynamics (QCD). Hadrons
 322 like proton and neutron have internal structure given that they are composed
 323 of two or more valence quarks⁵. Quarks have fractional electric charge which
 324 means that they are subject to electromagnetic interaction and in the case of the
 325 proton they should break apart due to electrostatic repulsion; however, quarks
 326 are held together inside the hadrons against their electrostatic repulsion by the
 327 “Strong Force” through the exchange of “gluons.” The analog to the electric
 328 charge is the “color charge”. Electrons and photons are elementary particles
 329 as quarks but they don’t carry color charge, therefore they are not subject to
 330 SI. The feynman diagram for gluon exchange between quarks is shown in figure
 331 2.4b.
- 332 ● *Weak interaction (WI)* described by the Weak theory (WT), is responsible for
 333 instance for the radioactive decay in atoms and proton-proton (pp) fusion within
 334 the sun. Quarks and leptons are the particles affected by the weak interaction
 335 and posses a property called “flavor charge” which can be changed by emitting
 336 or absorbing one weak force mediator; they comes in six flavors each (see 2.2.1).

⁵ particles made of four and five quarks are exotic states not so common

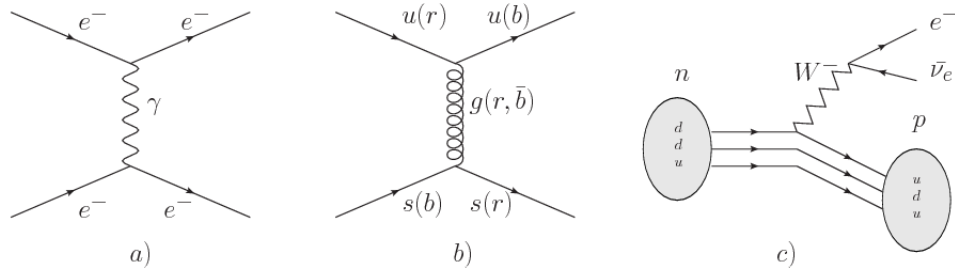


Figure 2.4: Feynman diagrams representing the interactions in SM; a) EI: e - e scattering; b) SI: gluon exchange between quarks ; c) WI: β -decay

337 There are three mediators of the “Weak force” known as “Z” boson in the case of
 338 electrically neutral changes and “ W^\pm ” bosons in the case of electrically charged
 339 changes. The “weak isospin” is the WI analog to electric charge in EI and color
 340 charge in SI and define how quarks and leptons are affected by the weak force.
 341 Figure 2.4c. shows the feynman diagram of β -decay where a newtron (n) is
 342 transformed in a proton (p) by emmiting a W^- particle. Since this thesis is in
 343 the frame of the electroweak interaction, a more detailed description of it will
 344 be given in section 2.3

- 345 • *Gravitational interaction (GI)* described by General Theory of Relativity (GR).
 346 It is responsible for the structure of galaxies and black holes as well as the
 347 expansion of the universe. As a classical theory, in the sense that it can be
 348 formulated without even appeal to the concept of quantization, it implies that
 349 the spacetime is a continuum and predictions can be made without limitation
 350 to the precision of the measurement tools which represent a direct contradiction
 351 of the quantum mechanics principles. Gravity is deterministic while quantum
 352 mechanics is probabilistic; despite that, efforts to develop a quantum theory of
 353 gravity have predicted the “graviton” as mediator of the Gravitational force⁶.

⁶ Actually a wide variety of theories have been developed in an attempt to describe gravity; some famous examples are string theory and supergravity.

| Interaction | Acts on | Relative strength | Range (m) | Mediators |
|-----------------------|--------------------------------|-------------------|------------|------------|
| Electromagnetic (QED) | Electrically charged particles | 10^{-2} | Infinite | Photon |
| Strong (QCD) | Quarks and gluons | 1 | 10^{-15} | Gluon |
| Weak (WI) | Leptons and quarks | 10^{-6} | 10^{-18} | W^\pm, Z |
| Gravitational (GI) | Massive particles | 10^{-39} | Infinite | Graviton |

Table 2.5: Fundamental interactions features [30].

354

355 Table 2.5 summarizes the main features of the fundamental interactions. The rela-
 356 tive strength of the fundamental forces reveals the meaning of strong and weak; in
 357 a context where the relative strength of the SI is 1, the EI is about hundred times
 358 weaker and WI is about million times weaker than the SI. A good description on
 359 how the relative strength and range of the fundamental interactions are calculated
 360 can be found in references [30, 31]. In the everyday life, only EI and GI are explicitly
 361 experienced due to the range of these interactions; i.e., at the human scale distances
 362 only EI and GI have appreciable effects, in contrast to SI which at distances greater
 363 than 10^{-15} m become negligible.

364

365 QED was built successfully on the basis of the classical electrodynamics theory (CED)
 366 of Maxwell and Lorentz, following theoretical and experimental requirements imposed
 367 by

- 368 • lorentz invariance: independence on the reference frame.
 369 • locallity: interacting fields are evaluated at the same space-time point to avoid
 370 action at a distance.
 371 • renormalizability: physical predictions are finite and well defined

372 • particle spectrum, symmetries and conservation laws already known must emerge
 373 from the theory.

374 • gauge invariance.

375 The gauge invariance requirement reflects the fact that the fundamental fields cannot
 376 be directly measured but associated fields which are the observables. Electric (“**E**”)
 377 and magnetic (“**B**”) fields in CED are associated with the electric scalar potential
 378 “V” and the vector potential “**A**”. In particular, **E** can be obtained by measuring
 379 the change in the space of the scalar potential (ΔV); however, two scalar potentials
 380 differing by a constant “f” correspond to the same electric field. The same happens in
 381 the case of the vector potential “**A**”; thus, different configurations of the associated
 382 fields result in the same set of values of the observables. The freedom in choosing
 383 one particular configuration is known as “gauge freedom”; the transformation law
 384 connecting two configurations is known as “gauge transformation” and the fact that
 385 the observables are not affected by a gauge transformation is called “gauge invariance”.

386 When the gauge transformation:

$$\begin{aligned} \mathbf{A} &\rightarrow \mathbf{A} - \nabla f \\ V &\rightarrow V - \frac{\partial f}{\partial t} \end{aligned} \tag{2.4}$$

387 is applied to Maxwell equations, they are still satisfied and the fields remain invariant.
 388 Thus, CED is invariant under gauge transformations and is called a “gauge theory”.
 389 The set of all gauge transformations form the “symmetry group” of the theory, which
 390 according to the group theory, has a set of “group generators”. The number of group
 391 generators determine the number of “gauge fields” of the theory.

392

393 As mentioned in the first lines of section 2.2, QED has one symmetry group ($U(1)$)
 394 with one group generator (the Q operator) and one gauge field (the electromagnetic
 395 field A^μ). In CED there is not a clear definition, beyond the historical convention, of
 396 which fields are the fundamental and which are the associated, but in QED it is clear
 397 that the fundamental field is A^μ . When a gauge theory is quantized, the gauge field
 398 is quantized and its quanta is called “gauge boson”. The word boson characterizes
 399 particles with integer spin which obvey Bose-einstein statistics.

400

401 As will be detailed in section 2.3, interactions between particles in a system can be
 402 obtained by considering first the Lagrangian density of free particles in the system,
 403 which of course is incomplete because the interaction terms have been left out, and
 404 demanding global phase transformation invariance. Global phase transformation in-
 405 variance means that a gauge transformation is performed identically to every point
 406 in the space⁷ and the Lagrangian remains invariant. Then, the global transformation
 407 is promoted to a local phase transformation (this time the gauge transformation de-
 408 pends on the position in space) and again invariance is required.

409

410 Due to the space dependence of the local tranformation, the Lagrangian density is
 411 not invariant anymore. In order to restate the gauge invariance, the gauge covariant
 412 derivative is introduced in the Lagrangian and with it the gauge field responsible for
 413 the interaction between particles in the system. The new Lagrangian density is gauge
 414 invariant, includes the interaction terms needed to account for the interactions and
 415 provide a way to explain the interaction between particles through the exchange of
 416 the gauge boson.

⁷ Here space corresponds to the 4-dimensional space i.e. space-time.

417 This recipe was used to build QED and the theories that aim to explain the funda-
 418 mental interactions.

419 **2.2.3 Gauge Bosons**

420 The importance of the gauge bosons comes from the fact that they are the force
 421 mediators or force carriers. The features of the gauge bosons reflect the features of
 422 the fields they represent; these fatures are extracted from the Lagrangian density
 423 used to describe the interactions. In section 2.3, it will be shown how the gauge
 424 bosons of the EI and WI emerge from the electroweak Lagrangian. The SI gauge
 425 bosons features are also extracted from the SI Lagrangian but it is not detailed in
 426 this document. The main features of the SM gauge bosons will be briefly presented
 427 below and summarized in table 2.6.

428 • **Photon.** EI occurs when the photon couples to (is exchanged between) particles
 429 carrying electric charge; however, the photon itself does not carry electric charge,
 430 therefore, there is no coupling between photons. Given that the photon is
 431 massless the EI is of infinite range, i.e., electrically charged particles interact
 432 even if they are located far away one from each other; this also implies that
 433 photons always move with the speed of light.

434 • **Gluon.** SI is mediated by gluons which, same as photons, are massless. They
 435 carry one unit of color charge and one unit of anticolor charge which means that
 436 gluons couple to other gluons. As a result, the range of the SI is not infinite
 437 but very short due to the attraction between gluons, giving rise to the “color
 438 confinement” which explains why color charged particles cannot be isolated but
 439 live within composited particles, like quarks inside protons.

440 • **W, Z.** The EWI mediators, W^\pm and Z, are massive which explains their short-
 441 range. Given that the WI is the only interaction that can change the flavor
 442 of the interacting particles, the W boson is the responsible for the nuclear
 443 transmutation where a neutron is converted in a proton or vice versa with the
 444 involvement of an electron and a neutrino (see figure 2.4c). The Z boson is the
 445 responsible of the neutral weak processes like neutrino elastic scattering where
 446 no electric charge but momentum transference is involved. WI gauge bosons
 447 carry isospin charge which makes possible the interaction between them.

| Interaction | Mediator | Electric charge (e) | Color charge | Weak Isospin | mass (GeV/c ²) |
|-----------------|---------------------|---------------------|--------------|--------------|----------------------------|
| Electromagnetic | Photon (γ) | 0 | No | 0 | 0 |
| Strong | Gluon (g) | 0 | Yes -octet | No | 0 |
| Weak | W^\pm | ± 1 | No | ± 1 | 80.385 ± 0.015 |
| | Z | 0 | No | 0 | 91.188 ± 0.002 |

Table 2.6: SM gauge bosons main features [21].

448

449 2.3 Electroweak unification and the Higgs 450 mechanism

451 Physicists dreams of building a theory that contains all the interactions in one single
 452 interaction, i.e., showing that at some scale in energy all the four fundamental in-
 453 teractions are unified and only one interaction emerges in a “Theory of everything”.
 454 The first sign of the feasibility of such unification comes from success in the con-
 455 struction of the CED. Einstein spent years trying to reach that dream, which by
 456 1920 only involved electromagnetism and gravity, with no success; however, a new
 457 partial unification was achieved in the 1960’s, when S.Glashow [14], A.Salam [15] and
 458 S.Weinberg [16] independently proposed that electromagnetic and weak interactions

459 are two manifestations of a more general interaction called “electroweak interaction
 460 (EWT).” QCD and EWT were developed in parallel and following the useful prescrip-
 461 tion provided by QED and the gauge invariance principles.

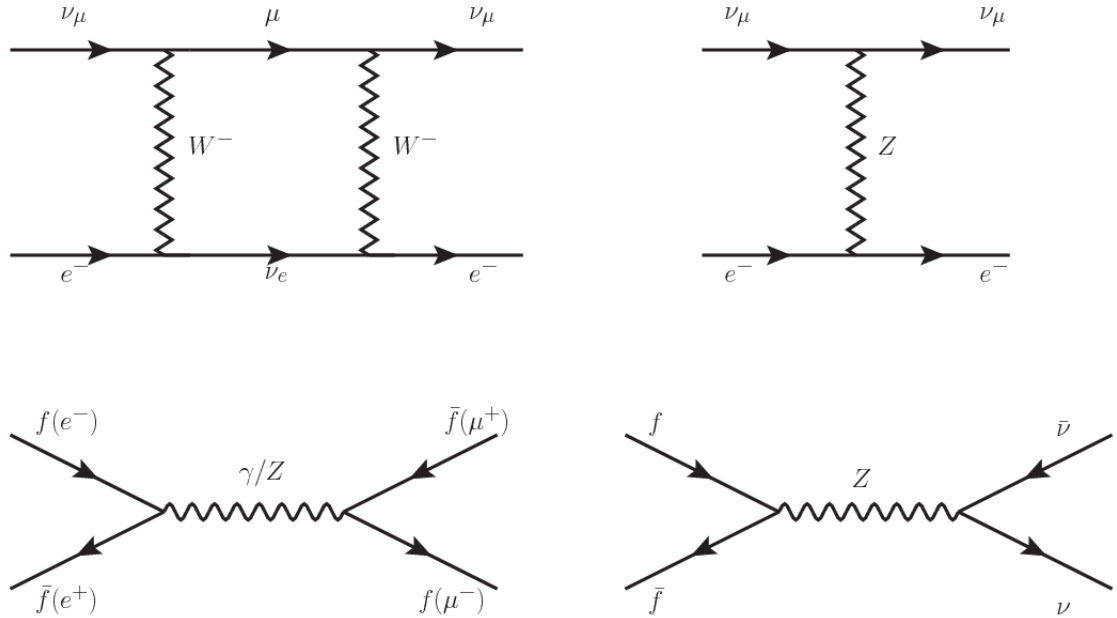


Figure 2.5: Top: $\nu_\mu - e^-$ scattering going through charged currents (left) and neutral currents (right). Bottom: neutral current processes for charged fermions (left) and involving neutrinos (right). While neutral current processes involving only charged fermions can proceed through EI or WI, those involving neutrinos can only proceed via WI.

462
 463 The theory of weak interactions was capable of explaining the β -decay and in general
 464 the processes mediated by W^\pm bosons. However, there were some processes like the
 465 “ $\nu_\mu - e$ scattering” which would require the exchange of two W bosons (see figure 2.5
 466 top diagrams) giving rise to divergent loop integrals and then non finite predictions.
 467 By including neutral currents involving fermions via the exchange of neutral bosons
 468 Z, those divergences are compensated and the predictions become realistic.
 469 Neutral weak interaction vertices conserve flavor in the same way as the electromag-
 470 netic vertices do, but additionally, the Z boson can couple to neutrinos which implies

471 that processes involving charged fermions can proceed through EI or WI but processes
 472 involving neutrinos can proceed only through WI.

473

474 The prescription to build a gauge theory of the WI consist of proposing a free field La-
 475 grangian density that includes the particles involved; next, by requesting invariance
 476 under global phase transformations first and generalizing to local phase transfor-
 477 mations invariance later, the conserved currents are identified and interactions are
 478 generated by introducing gauge fields. Given that the goal is to include the EI and
 479 WI in a single theory, the group symmetry considered should be a combination of
 480 $SU(2)_L$ and $U(1)_{em}$, however the latter cannot be used directly because the EI treat
 481 left and right-handed particles indistinctly in contrast to the former. Fortunately, the
 482 weak hypercharge, which is a combination of the weak isospin and the electric charge
 483 (eqn 2.2) is suitable to be used since it is conserved by the EI and WI. Thus, the
 484 symmetry group to be considered is

$$G \equiv SU(2)_L \otimes U(1)_Y \quad (2.5)$$

485 The following treatment applies to any of the fermion generations, but for simplicity
 486 the first generation of leptons will be considered [2, 3, 32, 33].

487

488 Given the first generation of leptons

$$\psi_1 = \begin{pmatrix} \nu_e \\ e^- \end{pmatrix}_L, \quad \psi_2 = \nu_{eR}, \quad \psi_3 = e_R^- \quad (2.6)$$

489 the charged fermionic currents are given by

$$J_\mu \equiv J_\mu^+ = \bar{\nu}_{eL} \gamma_\mu e_L, \quad J_\mu^\dagger \equiv J_\mu^- = \bar{e}_L \gamma_\mu \nu_{eL} \quad (2.7)$$

490 and the free Lagrangian is given by

$$\mathcal{L}_0 = \sum_{j=1}^3 i\bar{\psi}_j(x)\gamma^\mu\partial_\mu\psi_j(x). \quad (2.8)$$

491 Mass terms are included directly in the QED and QCD free Lagrangians since they
 492 preserve the invariance under the symmetry transformations involved which treat
 493 left-handed and right-handed similarly, however mass terms of the form

$$m_W^2 W_\mu^\dagger(x)W^\mu(x) + \frac{1}{2}m_Z^2 Z_\mu(x)Z^\mu(x) - m_e\bar{\psi}_e(x)\psi_e(x) \quad (2.9)$$

494 which represent the mass of W^\pm , Z and electrons, are not invariant under G trans-
 495 formations, therefore the gauge fields described by the EWI are in principle massless.

496

497 Experiments have shown that the gauge fields are not massless; however, they have
 498 to acquire mass through a mechanism compatible with the gauge invariance; that
 499 mechanism is known as the “Higgs mechanism” and will be considered later in this
 500 section. The global transformations in the combined symmetry group G can be
 501 written as

$$\begin{aligned} \psi_1(x) &\xrightarrow{G} \psi'_1(x) \equiv U_Y U_L \psi_1(x), \\ \psi_2(x) &\xrightarrow{G} \psi'_2(x) \equiv U_Y \psi_2(x), \\ \psi_3(x) &\xrightarrow{G} \psi'_3(x) \equiv U_Y \psi_3(x) \end{aligned} \quad (2.10)$$

502 where U_L represent the $SU(2)_L$ transformation acting only on the weak isospin dou-
 503 blet and U_Y represent the $U(1)_Y$ transformation acting on all the weak isospin mul-

504 triplets. Explicitly

$$U_L \equiv \exp\left(i\frac{\sigma_i}{2}\alpha^i\right), \quad U_Y \equiv \exp(iy_i\beta) \quad (i = 1, 2, 3) \quad (2.11)$$

505 with σ_i the Pauli matrices and y_i the weak hypercharges. In order to promote the
 506 transformations from global to local while keeping the invariance, it is required that
 507 $\alpha^i = \alpha^i(x)$, $\beta = \beta(x)$ and the replacement of the ordinary derivatives by the covariant
 508 derivatives

$$\begin{aligned} D_\mu \psi_1(x) &\equiv \left[\partial_\mu + ig\sigma_i W_\mu^i(x)/2 + ig'y_1 B_\mu(x) \right] \psi_1(x) \\ D_\mu \psi_2(x) &\equiv \left[\partial_\mu + ig'y_2 B_\mu(x) \right] \psi_2(x) \\ D_\mu \psi_3(x) &\equiv \left[\partial_\mu + ig'y_3 B_\mu(x) \right] \psi_3(x) \end{aligned} \quad (2.12)$$

509 introducing in this way four gauge fields, $W_\mu^i(x)$ and $B_\mu(x)$, in the process. The
 510 covariant derivatives (eqn 2.12) are required to transform in the same way as fermion
 511 fields $\psi_i(x)$ themselves, therefore, the gauge fields transform as:

$$\begin{aligned} B_\mu(x) &\xrightarrow{G} B'_\mu(x) \equiv B_\mu(x) - \frac{1}{g'} \partial_\mu \beta(x) \\ W_\mu^i(x) &\xrightarrow{G} W_\mu^{i\prime}(x) \equiv W_\mu^i(x) - \frac{i}{g} \partial_\mu \alpha_i(x) - \varepsilon_{ijk} \alpha_i(x) W_\mu^j(x). \end{aligned} \quad (2.13)$$

512 The G invariant version of the Lagrangian density 2.8 can be written as

$$\mathcal{L}_0 = \sum_{j=1}^3 i\bar{\psi}_j(x) \gamma^\mu D_\mu \psi_j(x) \quad (2.14)$$

513 where free massless fermion and gauge fields and fermion-gauge boson interactions

514 are included. The EWI Lagrangian density must additionally include kinetic terms
 515 for the gauge fields (\mathcal{L}_G) which are built from the field strengths, according to

$$B_{\mu\nu}(x) \equiv \partial_\mu B_\nu - \partial_\nu B_\mu \quad (2.15)$$

$$W_{\mu\nu}^i(x) \equiv \partial_\mu W_\nu^i(x) - \partial_\nu W_\mu^i(x) - g\varepsilon^{ijk}W_\mu^j W_\nu^k \quad (2.16)$$

516 the last term in eqn. 2.16 is added in order to hold the gauge invariance; therefore,

$$\mathcal{L}_G = -\frac{1}{4}B_{\mu\nu}(x)B^{\mu\nu}(x) - \frac{1}{4}W_{\mu\nu}^i(x)W_i^{\mu\nu}(x) \quad (2.17)$$

517 which contains not only the free gauge fields contributions, but also the gauge fields
 518 self-interactions and interactions among them.

519 The three weak isospin conserved currents resulting from the $SU(2)_L$ symmetry are
 520 given by

$$J_\mu^i(x) = \frac{1}{2}\bar{\psi}_1(x)\gamma_\mu\sigma^i\psi_1(x) \quad (2.18)$$

521 while the weak hypercharge conserved current resulting from the $U(1)_Y$ symmetry is
 522 given by

$$J_\mu^Y = \sum_{j=1}^3 \bar{\psi}_j(x)\gamma_\mu y_j\psi_j(x) \quad (2.19)$$

523 In order to evaluate the electroweak interactions modeled by an isos triplet field W_μ^i
 524 which couples to isospin currents J_μ^i with strength g and additionally the singlet
 525 field B_μ which couples to the weak hypercharge current J_μ^Y with strength $g'/2$. The
 526 interaction Lagrangian density to be considered is

$$\mathcal{L}_I = -g J^{i\mu}(x) W_\mu^i(x) - \frac{g'}{2} J^{Y\mu}(x) B_\mu(x) \quad (2.20)$$

527 Note that the weak isospin currents are not the same as the charged fermionic currents
 528 that were used to describe the WI (eqn 2.7), since the weak isospin eigenstates are
 529 not the same as the mass eigenstates, but they are closely related

$$J_\mu = \frac{1}{2}(J_\mu^1 + iJ_\mu^2), \quad J_\mu^\dagger = \frac{1}{2}(J_\mu^1 - iJ_\mu^2). \quad (2.21)$$

530 The same happens with the gauge fields W_μ^i which are related to the mass eigenstates
 531 W^\pm by

$$W_\mu^+ = \frac{1}{\sqrt{2}}(W_\mu^1 - iW_\mu^2), \quad W_\mu^- = \frac{1}{\sqrt{2}}(W_\mu^1 + iW_\mu^2). \quad (2.22)$$

532 The fact that there are three weak isospin conserved currents is an indication that in
 533 addition to the charged fermionic currents, which couple charged to neutral leptons,
 534 there should be a neutral fermionic current that couples neutral fermions or electri-
 535 cally charged fermions that have the same electric charge and thus electric charge
 536 change is not implied. The third weak isospin current contains a term that is simi-
 537 lar to the electromagnetic current (j_μ^{em}), indicating that there is a relation between
 538 them and resembling the Gell-Mann-Nishijima formula 2.2 adapted to electroweak
 539 interactions

$$Q = T_3 + \frac{Y_W}{2}. \quad (2.23)$$

540 Just as Q generates the $U(1)_{em}$ symmetry, the weak hypercharge generates the $U(1)_Y$
 541 symmetry as said before. It is possible to write the relationship in terms of the currents
 542 as

$$j_\mu^{em} = J_\mu^3 + \frac{1}{2} J_\mu^Y. \quad (2.24)$$

543 The neutral gauge fields W_μ^3 and B_μ cannot be directly identified with the Z and the
 544 photon fields since the photon interacts similarly with left and right-handed fermions;
 545 however, they are related through a linear combination given by

$$\begin{aligned} A_\mu &= B_\mu \cos \theta_W + W_\mu^3 \sin \theta_W \\ Z_\mu &= -B_\mu \sin \theta_W + W_\mu^3 \cos \theta_W \end{aligned} \quad (2.25)$$

546 where θ_W is known as the “Weinberg angle.” The interaction Lagrangian is now given
 547 by

$$\mathcal{L}_I = -\frac{g}{\sqrt{2}}(J^\mu W_\mu^+ + J^{\mu\dagger} W_\mu^-) - \left(g \sin \theta_W J_\mu^3 + g' \cos \theta_W \frac{J_\mu^Y}{2} \right) A^\mu - \left(g \cos \theta_W J_\mu^3 - g' \sin \theta_W \frac{J_\mu^Y}{2} \right) Z^\mu \quad (2.26)$$

548 the first term is the weak charged current interaction, while the second term is the
 549 electromagnetic interaction under the condition

$$g \sin \theta_W = g' \cos \theta_W = e, \quad \frac{g'}{g} = \tan \theta_W \quad (2.27)$$

550 contained in the eqn.2.24; the third term is the neutral weak current.

551 Note that the neutral fields transformation given by the eqn. 2.25 can be written in
 552 terms of the coupling constants g and g' as:

$$A_\mu = \frac{g' W_\mu^3 + g B_\mu}{\sqrt{g^2 + g'^2}}, \quad Z_\mu = \frac{g W_\mu^3 - g' B_\mu}{\sqrt{g^2 + g'^2}} \quad (2.28)$$

553 So far, the Lagrangian density describing the non-massive EWI is:

$$\mathcal{L}_{nmEWI} = \mathcal{L}_0 + \mathcal{L}_G \quad (2.29)$$

554 where fermion and gauge fields have been considered massless because their regular
 555 mass terms are manifestly non invariant under G transformations; therefore, masses
 556 have to be generated in a gauge invariant way. The mechanism by which this goal is
 557 achieved is known as the “Higgs mechanism” and is closely connected to the concept
 558 of “spontaneous symmetry breaking.”

559 2.3.1 Spontaneous symmetry breaking

560 Figure 2.6 left shows a steel nail (top) which is subject to an external force; the form
 561 of the potential energy is also shown (bottom).

562 Before reaching the critical force value, the system has rotational symmetry with re-
 563 spect to the nail axis; however, after the critical force value is reached the nail buckles
 564 (top right). The form of the potential energy (bottom right) changes, preserving its
 565 rotational symmetry although its minima does not exhibit that rotational symmetry
 566 any longer. Right before the nail buckles there is no indication of the direction the
 567 nail will bend because any of the directions are equivalent, but once the nail bent,
 568 choosing a direction, an arbitrary minimal energy state (ground state) is selected and
 569 it does not share the system rotational symmetry. This mechanism for reaching an
 570 asymmetric ground state is known as “*spontaneous symmetry breaking (SSB)*”.

571 The lesson from this analysis is that the way to introduce the SSB mechanism into a
 572 system is by adding the appropriate potential to it.

573

574 Figure 2.7 shows a plot of the potential $V(\phi)$ in the case of a scalar field ϕ

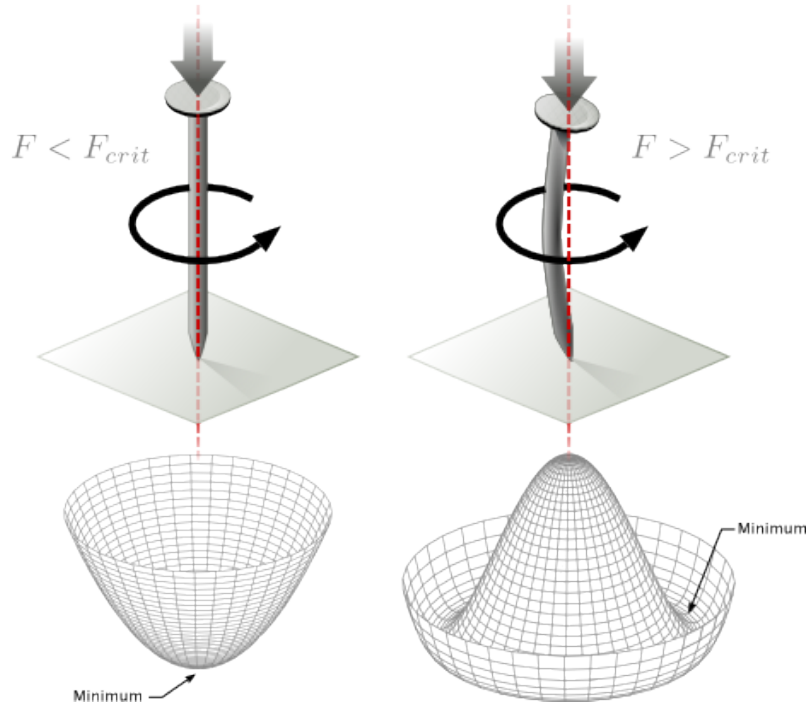


Figure 2.6: Spontaneous symmetry breaking mechanism. The steel nail, subject to an external force (top left), has rotational symmetry with respect to its axis. When the external force overcomes a critical value the nail buckles (top right) choosing a minimal energy state (ground state) and thus “*breaking spontaneously the rotational symmetry*”. The potential energy (bottom) changes but holds the rotational symmetry; however, an infinite number of asymmetric ground states are generated and circularly distributed in the bottom of the potential [34].

$$V(\phi) = \mu^2 \phi^\dagger \phi + \lambda (\phi^\dagger \phi)^2 \quad (2.30)$$

- 575 If $\mu^2 > 0$ the potential has only one minimum at $\phi = 0$ and describes a scalar field
 576 with mass μ . If $\mu^2 < 0$ the potential has a local maximum at $\phi = 0$ and two minima
 577 at $\phi = \pm\sqrt{-\mu^2/\lambda}$ which enables the SSB mechanism to work.
 578 In the case of a complex scalar field $\phi(x)$

$$\phi(x) = \frac{1}{\sqrt{2}}(\phi_1 + i\phi_2) \quad (2.31)$$

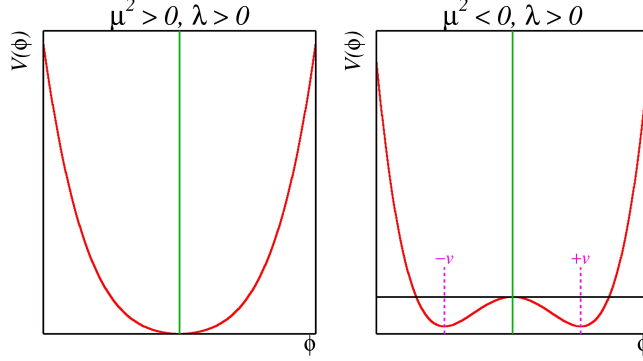


Figure 2.7: Shape of the potential $V(\phi)$ for $\lambda > 0$ and: $\mu^2 > 0$ (left) and $\mu^2 < 0$ (right). The case $\mu^2 < 0$ corresponds to the potential suitable for introducing the SSB mechanism by choosing one of the two ground states which are connected via reflection symmetry. [34].

579 the Lagrangian (invariant under global $U(1)$ transformations) is given by

$$\mathcal{L} = (\partial_\mu \phi)^\dagger (\partial^\mu \phi) - V(\phi), \quad V(\phi) = \mu^2 \phi^\dagger \phi + \lambda (\phi^\dagger \phi)^2 \quad (2.32)$$

580 where an appropriate potential has been added in order to introduce the SSB.

581 As seen in figure 2.8, the potential has now an infinite number of minima circularly
 582 distributed along the ξ -direction which makes possible the occurrence of the SSB by
 583 choosing an arbitrary ground state; for instance, $\xi = 0$, i.e. $\phi_1 = v, \phi_2 = 0$

$$\phi_0 = \frac{v}{\sqrt{2}} \exp(i\xi) \xrightarrow{\text{SSB}} \phi_0 = \frac{v}{\sqrt{2}} \quad (2.33)$$

584 As usual, excitations over the ground state are studied by making an expansion about
 585 it; thus, the excitation can be parametrized as:

$$\phi(x) = \frac{1}{\sqrt{2}} (v + \eta(x) + i\xi(x)) \quad (2.34)$$

586 which when substituted into eqn. 2.32 produces a Lagrangian in terms of the new
 587 fields η and ξ

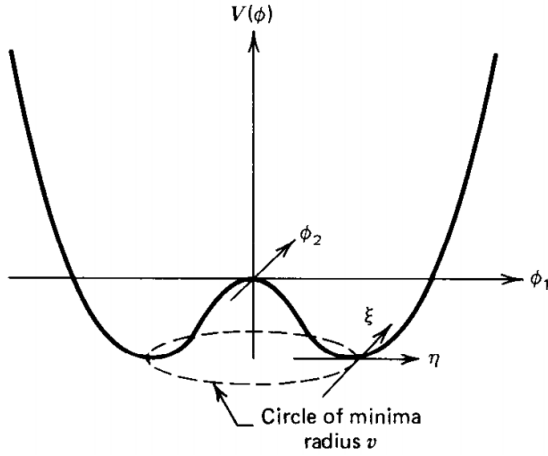


Figure 2.8: Potential for complex scalar field. There is a circle of minima of radius v along the ξ -direction [3].

$$\mathcal{L}' = \frac{1}{2}(\partial_\mu \xi)^2 + \frac{1}{2}(\partial_\mu \eta)^2 + \mu^2 \eta^2 - V(\phi_0) - \lambda v \eta (\eta^2 + \xi^2) - \frac{\lambda}{4}(\eta^2 + \xi^2)^2 \quad (2.35)$$

588 where the last two terms represent the interactions and self-interaction between the
 589 two fields η and ξ . The particular feature of the SSB mechanism is revealed when
 590 looking to the first three terms of \mathcal{L}' . Before the SSB, only the massless ϕ field is
 591 present in the system; after the SSB there are two fields of which the η -field has
 592 acquired mass $m_\eta = \sqrt{-2\mu^2}$ while the ξ -field is still massless (see figure 2.9).
 593 Thus, *the SSB mechanism serves as a method to generate mass but as a side effect a*
 594 *massless field is introduced in the system.* This fact is known as the Goldstone theorem
 595 and states that a massless scalar field appears in the system for each continuous
 596 symmetry spontaneously broken. Another version of the Goldstone theorem states
 597 that “*if a Lagrangian is invariant under a continuous symmetry group G , but the*
 598 *vacuum is only invariant under a subgroup $H \subset G$, then there must exist as many*
 599 *massless spin-0 particles (Nambu-Goldstone bosons) as broken generators.*” [33] The
 600 Nambu-Goldstone boson can be understood considering that the potential in the ξ -

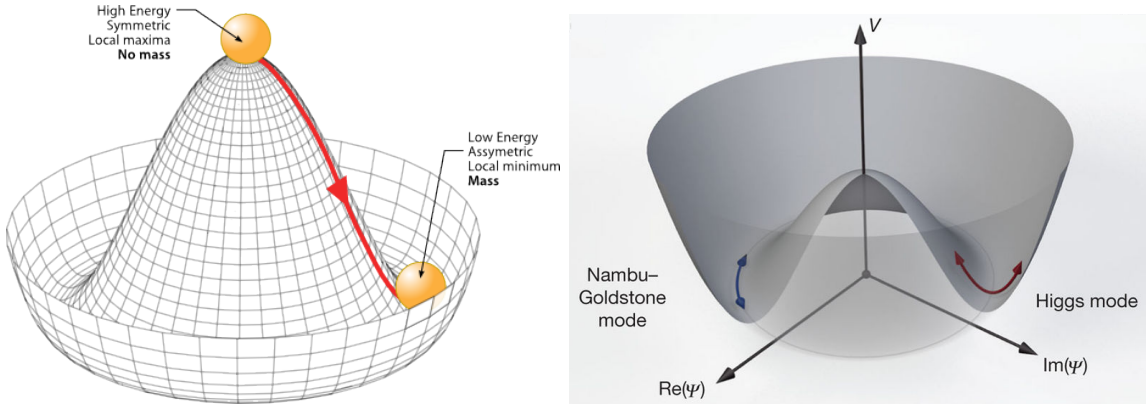


Figure 2.9: SSB mechanism for a complex scalar field [34, 35].

601 direction is flat so excitations in that direction are not energy consuming and thus
602 represent a massless state.

603 2.3.2 Higgs mechanism

604 When the SSB mechanism is introduced in the formulation of the EWI in an attempt
605 to generate the mass of the so far massless gauge bosons and fermions, an interesting
606 effect is revealed. In order to keep the G symmetry group invariance and generate
607 the mass of the EW gauge bosons, a G invariant Lagrangian density (\mathcal{L}_S) has to be
608 added to the non massive EWI Lagrangian (eqn. 2.29)

$$\mathcal{L}_S = (D_\mu \phi)^\dagger (D^\mu \phi) - \mu^2 \phi^\dagger \phi - \lambda (\phi^\dagger \phi)^2, \quad \lambda > 0, \mu^2 < 0 \quad (2.36)$$

$$D_\mu \phi = \left(i\partial_\mu - g \frac{\sigma_i}{2} W_\mu^i - g' \frac{Y}{2} B_\mu \right) \phi \quad (2.37)$$

609 ϕ has to be an isospin doublet of complex scalar fields so it preserves the G invariance;
610 thus ϕ can be defined as:

$$\phi = \begin{pmatrix} \phi^+ \\ \phi^0 \end{pmatrix} \equiv \frac{1}{\sqrt{2}} \begin{pmatrix} \phi_1 + i\phi_2 \\ \phi_3 + i\phi_4 \end{pmatrix}. \quad (2.38)$$

611 The minima of the potential are defined by

$$\phi^\dagger \phi = \frac{1}{2} (\phi_1^2 + \phi_2^2 + \phi_3^2 + \phi_4^2) = -\frac{\mu^2}{2\lambda}. \quad (2.39)$$

612 The choice of the ground state is critical. By choosing a ground state, invariant under
 613 $U(1)_{em}$ gauge symmetry, the photon will remain massless and the W^\pm and Z bosons
 614 masses will be generated which is exactly what is needed. In that sense, the best
 615 choice corresponds to a weak isospin doublet with $T_3 = -1/2$, $Y_W = 1$ and $Q = 0$
 616 which defines a ground state with $\phi_1 = \phi_2 = \phi_4$ and $\phi_3 = v$:

$$\phi_0 \equiv \frac{1}{\sqrt{2}} \begin{pmatrix} 0 \\ v \end{pmatrix}, \quad v^2 \equiv -\frac{\mu^2}{\lambda}. \quad (2.40)$$

617 where the vacuum expectation value v is fixed by the Fermi coupling G_F according
 618 to $v = (\sqrt{2}G_F)^{1/2} \approx 246$ GeV.

619 The G symmetry has been broken and three Nambu-Goldstone bosons will appear.
 620 The next step is to expand ϕ about the chosen ground state as:

$$\phi(x) = \frac{1}{\sqrt{2}} \exp\left(\frac{i}{v} \sigma_i \theta^i(x)\right) \begin{pmatrix} 0 \\ v + H(x) \end{pmatrix} \approx \frac{1}{\sqrt{2}} \begin{pmatrix} \theta_1(x) + i\theta_2(x) \\ v + H(x) - i\theta_3(x) \end{pmatrix} \quad (2.41)$$

621 to describe fluctuations from the ground state ϕ_0 . The fields $\theta_i(x)$ represent the
 622 Nambu-Goldstone bosons while $H(x)$ is known as “higgs field.” The fundamental
 623 feature of the parametrization used is that the dependence on the $\theta_i(x)$ fields is
 624 factored out in a global phase that can be eliminated by taking the physical “unitary

625 gauge” $\theta_i(x) = 0$. Therefore the expansion about the ground state is given by:

$$\phi(x) \frac{1}{\sqrt{2}} \begin{pmatrix} 0 \\ v + H(x) \end{pmatrix} \quad (2.42)$$

626 which when substituted into \mathcal{L}_S (eqn. 2.36) results in a Lagrangian containing the now
 627 massive three gauge bosons W^\pm, Z , one massless gauge boson (photon) and the new
 628 Higgs field (H). The three degrees of freedom corresponding to the Nambu-Goldstone
 629 bosons are now integrated into the massive gauge bosons as their longitudinal polar-
 630 izations which were not available when they were massless particles. The effect by
 631 which vector boson fields acquire mass after an spontaneous symmetry breaking but
 632 without an explicit gauge invariance breaking is known as the “*Higgs mechanism*.”
 633 The mechanism was proposed by three independent groups: F.Englert and R.Brout
 634 in August 1964 [36], P.Higgs in October 1964 [37] and G.Guralnik, C.Hagen and
 635 T.Kibble in November 1964 [38]; however, its importance was not realized until
 636 S.Glashow [14], A.Salam [15] and S.Weinberg [16], independently, proposed that elec-
 637 tromagnetic and weak interactions are two manifestations of a more general interac-
 638 tion called “electroweak interaction” in 1967.

639 2.3.3 Masses of the gauge bosons

640 The mass of the gauge bosons is extracted by evaluating the kinetic part of Lagrangian
 641 \mathcal{L}_S in the ground state (known also as the vacuum expectation value), i.e.,

$$\left| \left(\partial_\mu - ig \frac{\sigma_i}{2} W_\mu^i - i \frac{g'}{2} B_\mu \right) \phi_0 \right|^2 = \left(\frac{1}{2} vg \right)^2 W_\mu^+ W^{-\mu} + \frac{1}{8} v^2 (W_\mu^3, B_\mu) \begin{pmatrix} g^2 & -gg' \\ -gg' & g'^2 \end{pmatrix} \begin{pmatrix} W^{3\mu} \\ B^\mu \end{pmatrix} \quad (2.43)$$

642 comparing with the typical mass term for a charged boson $M_W^2 W^+ W^-$

$$M_W = \frac{1}{2} v g. \quad (2.44)$$

The second term in the right side of the eqn.2.43 comprises the masses of the neutral bosons, but it needs to be written in terms of the gauge fields Z_μ and A_μ in order to be compared to the typical mass terms for neutral bosons, therefore using eqn. 2.28

$$\begin{aligned} \frac{1}{8} v^2 [g^2 (W_\mu^3)^2 - 2gg' W_\mu^3 B^\mu + g'^2 B_\mu^2] &= \frac{1}{8} v^2 [g W_\mu^3 - g' B_\mu]^2 + 0[g' W_\mu^3 + g B_\mu]^2 \\ &= \frac{1}{8} v^2 [\sqrt{g^2 + g'^2} Z_\mu]^2 + 0[\sqrt{g^2 + g'^2} A_\mu]^2 \end{aligned} \quad (2.45)$$

643 and then

$$M_Z = \frac{1}{2} v \sqrt{g^2 + g'^2}, \quad M_A = 0 \quad (2.46)$$

644 2.3.4 Masses of the fermions

645 The lepton mass terms can be generated by introducing a gauge invariant Lagrangian

646 term describing the Yukawa coupling between the lepton field and the Higgs field

$$\mathcal{L}_{Yl} = -G_l \left[(\bar{\nu}_l, \bar{l})_L \begin{pmatrix} \phi^+ \\ \phi^0 \end{pmatrix} l_R + \bar{l}_R (\phi^-, \bar{\phi}^0) \begin{pmatrix} \nu_l \\ l \end{pmatrix}_L \right], \quad l = e, \mu, \tau. \quad (2.47)$$

647 After the SSB and replacing the usual field expansion about the ground state (eqn.2.40)

648 into \mathcal{L}_{Yl} , the mass term arises

$$\mathcal{L}_{Yl} = -m_l (\bar{l}_L l_R + \bar{l}_R l_L) - \frac{m_l}{v} (\bar{l}_L l_R + \bar{l}_R l_L) H = -m_l \bar{l} l \left(1 + \frac{H}{v} \right) \quad (2.48)$$

649

$$m_l = \frac{G_l}{\sqrt{2}} v \quad (2.49)$$

650 where the additional term represents the lepton-Higgs interaction. The quark masses
 651 are generated in a similar way as lepton masses but for the upper member of the
 652 quark doublet a different Higgs doublet is needed:

$$\phi_c = -i\sigma_2\phi^* = \begin{pmatrix} -\bar{\phi}^0 \\ \phi^- \end{pmatrix}. \quad (2.50)$$

653 Additionally, given that the quark isospin doublets are not constructed in terms of
 654 the mass eigenstates but in terms of the flavor eigenstates, as shown in table 2.4, the
 655 coupling parameters will be related to the CKM matrix elements; thus the quark
 656 Lagrangian is given by:

$$\mathcal{L}_{Yq} = -G_d^{i,j}(\bar{u}_i, \bar{d}'_i)_L \begin{pmatrix} \phi^+ \\ \phi^0 \end{pmatrix} d_{jR} - G_u^{i,j}(\bar{u}_i, \bar{d}'_i)_L \begin{pmatrix} -\bar{\phi}^0 \\ \phi^- \end{pmatrix} u_{jR} + h.c. \quad (2.51)$$

657 with $i,j=1,2,3$. After SSB and expansion about the ground state, the diagonal form
 658 of \mathcal{L}_{Yq} is:

$$\mathcal{L}_{Yq} = -m_d^i \bar{d}_i d_i \left(1 + \frac{H}{v} \right) - m_u^i \bar{u}_i u_i \left(1 + \frac{H}{v} \right) \quad (2.52)$$

659 Fermion masses depend on arbitrary couplings G_l and $G_{u,d}$ and are not predicted by
 660 the theory.

661 2.3.5 The Higgs field

662 After the characterization of the fermions and gauge bosons as well as their interac-
 663 tions, it is necessary to characterize the Higgs field itself. The Lagrangian \mathcal{L}_S in eqn.

664 2.36 written in terms of the gauge bosons is given by

$$\mathcal{L}_S = \frac{1}{4} \lambda v^4 + \mathcal{L}_H + \mathcal{L}_{HV} \quad (2.53)$$

665 $\mathcal{L}_H = \frac{1}{2} \partial_\mu H \partial^\mu H - \frac{1}{2} m_H^2 H^2 - \frac{1}{2v} m_H^2 H^3 - \frac{1}{8v^2} m_H^2 H^4 \quad (2.54)$

666 $\mathcal{L}_{HV} = m_H^2 W_\mu^+ W^{\mu-} \left(1 + \frac{2}{v} H + \frac{2}{v^2} H^2 \right) + \frac{1}{2} m_Z^2 Z_\mu Z^\mu \left(1 + \frac{2}{v} H + \frac{2}{v^2} H^2 \right) \quad (2.55)$

667 The mass of the Higgs boson is deduced as usual from the mass term in the Lagrangian
 668 resulting in:

$$m_H = \sqrt{-2\mu^2} = \sqrt{2\lambda}v \quad (2.56)$$

669 however, it too is not predicted by the theory. The experimental efforts to find the
 670 Higgs boson, carried out by the CMS and ATLAS experiments⁸, gave great results
 671 by July of 2012 when the discovery of a new particles was announced and which
 672 is compatible with the Higgs boson predicted by the electroweak theory [39, 40].
 673 Although at the announcement time there were some reservations about calling the
 674 new particle the “Higgs boson”, today this name is widely accepted. The result of
 675 the measurement of the Higgs mass reported by both experiments [41] is in table 2.7.

| Property | Value |
|----------------------------|--------------------------------------|
| Electric charge | 0 |
| Colour charge | 0 |
| Spin | 0 |
| Weak isospin | -1/2 |
| Weak hypercharge | 1 |
| Parity | 1 |
| Mass (GeV/c ²) | 125.09 ± 0.21 (stat.) ± 0.11 (syst.) |

Table 2.7: Higgs boson properties. Higgs mass is not predicted by the theory and the value here corresponds to the experimental measurement.

676

⁸ CMS stands for Compact Muon Solenoid; ATLAS stand for A Toroidal LHC Apparatus. Both are general experiments held at the Large Hadron Collider(LHC)

677 2.3.6 Higgs boson production mechanisms at LHC.

At LHC, Higgs boson is produced as a result of the collision of two counter-rotating protons beams. A detailed description of the LHC machine will be presented in the chapter 3. “The total cross section” is the parameter that quantify the number of pp collisions that happen when a number of protons are fired at each other. Different results can be obtained after a pp collision and for each one the “cross section” is defined as the number of pp collisions that conclude in that particular result with respect to the number of protons fired at each other.

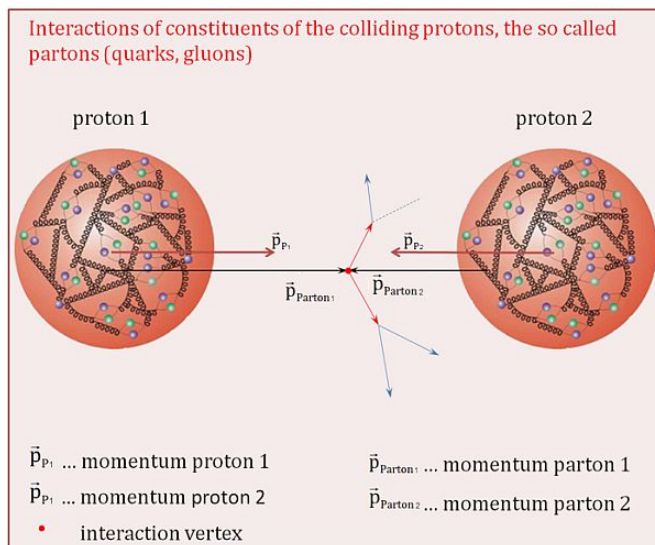


Figure 2.10: Proton-proton collision. Protons are composed of 3 valence quarks, a sea of quarks and gluons; therefore in a proton-proton collision, quarks and gluons are those who collide. [45].

684

685 Protons are composed of quarks and these quarks are bound by gluons; however, what
686 is commonly called the quark content of the proton makes reference to the valence
687 quarks. A sea of quarks and gluons is also present inside the proton as represented
688 in figure 2.10. In a proton-proton (pp) collision, the constituents (quarks and gluons)
689 are those who collide. The pp cross section depends on the momentum of the colliding
690 particles, reason for which it is needed to know how the momentum is distributed

691 inside the proton. Quarks and gluons are known as partons and the functions that
 692 describes how the proton momentum is distributed among partons inside it are called
 693 “parton distribution functions (PDFs)”; PDFs are determined from experimental data
 694 obtained in experiments where the internal structure of hadrons is tested.

695 In addition, in physics, a common approach to study complex systems consists in
 696 starting with a simpler version of them, for which a well known description is available,
 697 and add an additional “perturbation” which represent a small deviation from the
 698 known behavior. If the perturbation is small enough, the physical quantities associated
 699 with the perturbed system are expressed as a series of corrections to those of the
 700 simpler system; therefore, the more terms are considered in the series (the higher
 701 order in the perturbation series), the more precise is the the description of the complex
 702 system.

703 This thesis explore the Higgs production at LHC; therefore the overview presented
 704 here will be oriented specifically to the production mechanisms after pp collisions at
 705 LHC.

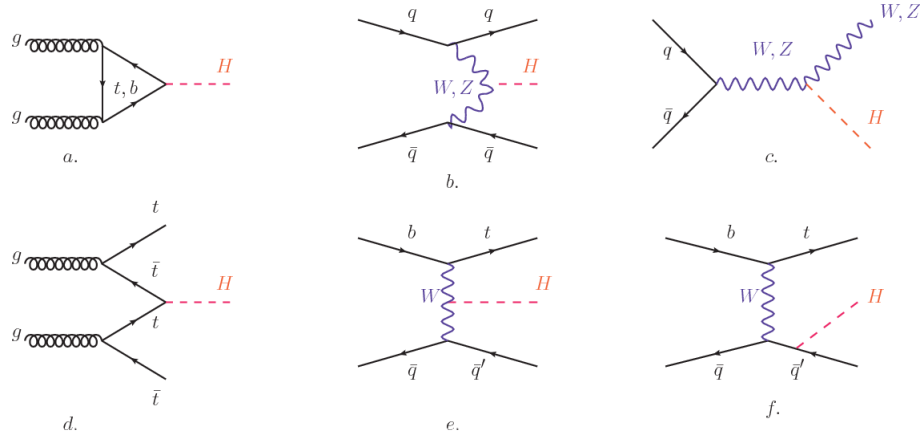


Figure 2.11: Main Higgs production mechanism Feynman diagrams. a. gluon-gluon fusion, b. vector boson fusion (VBF), c. Higgs-strahlung, d. Associated production with a top or bottom quark pair, e-f. associated production with a single top quark.

706 Figure 2.11 shows the Feynman diagrams for the leading order (first order) Higgs

707 production processes at LHC, while the cross section for Higgs production as a func-
 708 tion of the center of mass-energy (\sqrt{s}) for pp collisions is showed in figure 2.12 left.
 709 The tags NLO (next to leading order), NNLO (next to next to leading order) and
 710 N3LO (next to next to next to leading order) make reference to the order at which
 711 the perturbation series have been considered.

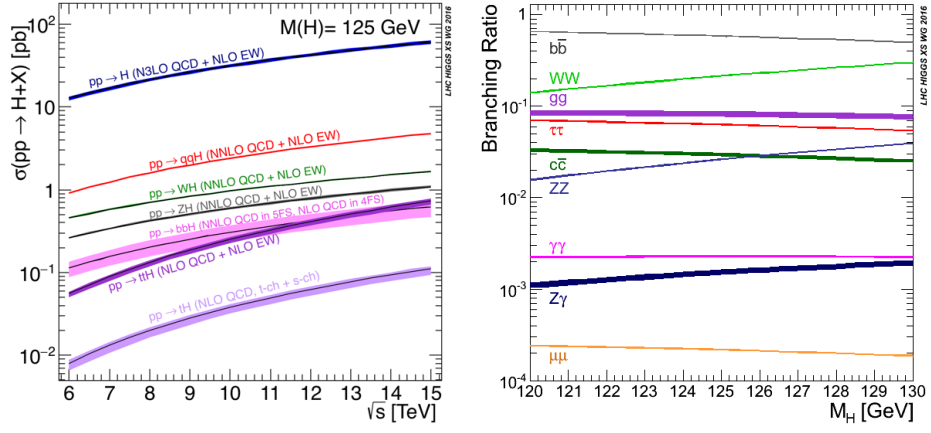


Figure 2.12: Higgs production cross sections (left) and decay branching ratios (right) for the main mechanisms. The VBF is indicated as $q\bar{q}H$ [42].

712 As shown in eqns 2.47, 2.51 and 2.55, the strength of the Higgs-fermion interaction
 713 is proportional to the fermion mass while the strength of the Higgs-gauge boson
 714 interaction is proportional to the square of the gauge boson mass, which implies
 715 that the Higgs production and decay mechanisms are dominated by couplings $H -$
 716 (W, Z, t, b, τ) .

717 The main production mechanism is the gluon fusion (figure 2.11a and $pp \rightarrow H$ in figure
 718 2.12) given that gluons carry the highest fraction of momentum of the protons in pp
 719 colliders. Since the Higgs boson does not couple to gluons, the mechanism proceeds
 720 through the exchange of a virtual top-quark loop given that for it the coupling is
 721 the biggest. Note that in this process, the Higgs boson is produced alone, which
 722 makes this mechanism experimentally clean when combined with the two-photon or

723 the four-lepton decay channels (see section 2.3.7).

724 Vector boson fusion (figure 2.11b and $pp \rightarrow qqH$ in figure 2.12) has the second largest
 725 production cross section. The scattering of two fermions is mediated by a weak
 726 gauge boson which later emits a Higgs boson. In the final state, the two fermions
 727 tend to be located in a particular region of the detector which is used as a signature
 728 when analyzing the datasets provided by the experiments. More details about how
 729 to identify events of interest in an analysis will be given in chapter 4.

730 The next production mechanism is Higgs-strahlung (figure 2.11c and $pp \rightarrow WH, pp \rightarrow$
 731 ZH in figure 2.12) where two fermions annihilate to form a weak gauge boson. If the
 732 initial fermions have enough energy, the emergent boson eventually will emit a Higgs
 733 boson.

734 The associated production with a top or bottom quark pair and the associated pro-
 735 duction with a single top quark (figure 2.11d-f and $pp \rightarrow bbH, pp \rightarrow t\bar{t}H, pp \rightarrow tH$
 736 in figure 2.12) have a smaller cross section than the main three mechanisms above,
 737 but they provide a good opportunity to test the Higgs-top coupling. The analysis
 738 reported in this thesis is developed using these production mechanisms. A detailed
 739 description of the tH mechanism will be given in section 2.4.

740 2.3.7 Higgs decay channels

741 When a particle can decay through several modes, also known as channels, the
 742 probability of decaying through a given channel is quantified by the “branching ratio
 743 (BR)” of the decay channel; thus, the BR is defined as the ratio of number of decays
 744 going through that given channel to the total number of decays. In regard to the
 745 Higgs boson decay, the BR can be predicted with accuracy once the Higgs mass is
 746 known [43, 44]. In figure 2.12 right, a plot of the BR as a function of the Higgs mass

747 is presented. The largest predicted BR corresponds to the $b\bar{b}$ pair decay channel (see
 748 table 2.8).

| Decay channel | Branching ratio | Rel. uncertainty |
|------------------------------|-----------------------|------------------|
| $H \rightarrow b\bar{b}$ | 5.84×10^{-1} | $+3.2\% - 3.3\%$ |
| $H \rightarrow W^+W^-$ | 2.14×10^{-1} | $+4.3\% - 4.2\%$ |
| $H \rightarrow \tau^+\tau^-$ | 6.27×10^{-2} | $+5.7\% - 5.7\%$ |
| $H \rightarrow ZZ$ | 2.62×10^{-2} | $+4.3\% - 4.1\%$ |
| $H \rightarrow \gamma\gamma$ | 2.27×10^{-3} | $+5.0\% - 4.9\%$ |
| $H \rightarrow Z\gamma$ | 1.53×10^{-3} | $+9.0\% - 8.9\%$ |
| $H \rightarrow \mu^+\mu^-$ | 2.18×10^{-4} | $+6.0\% - 5.9\%$ |

Table 2.8: Predicted branching ratios and the relative uncertainty for a SM Higgs boson with $m_H = 125 GeV/c^2$. [21]

749

750 2.4 Associated Production of Higgs Boson and 751 Single Top Quark.

752 Associated production of Higgs boson have been extensively studied [46–50]. While
 753 measurements of the main Higgs production mechanisms rates are sensitive to the
 754 strength of the Higgs coupling to W boson or top quark, they are not sensitive to the
 755 relative sign between the two couplings. In this thesis, the Higgs boson production
 756 mechanism explored is the associated production with a single top quark (th) which
 757 offers sensitiveness to the relative sign of the Higgs couplings to W boson and to top
 758 quark. The description given here is based on the reference [48]

759

760 A process where two incoming particles interact and produce a final state with two
 761 particles can proceed in three ways also called channels (see, for instance, figure 2.13

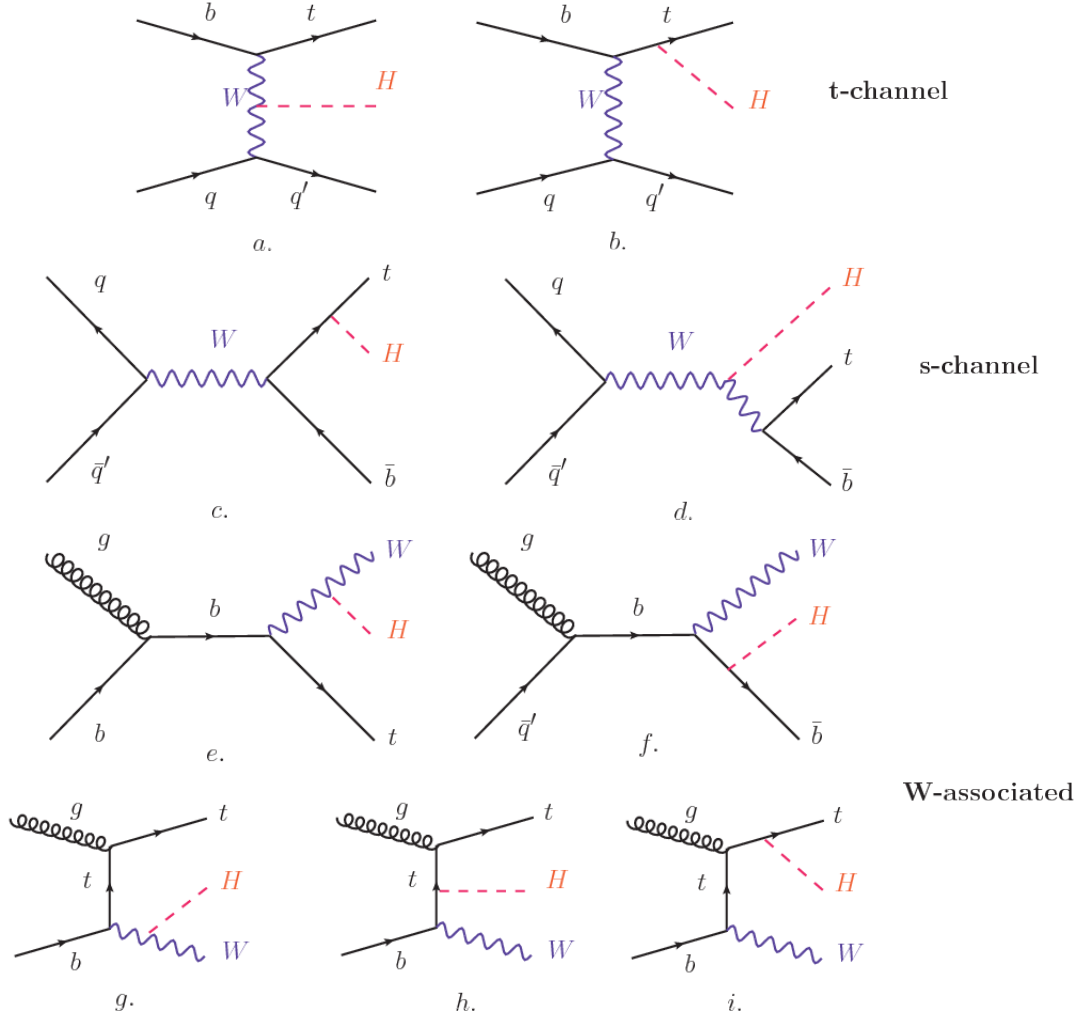


Figure 2.13: Associated higgs production mechanism Feynman diagrams. a.,b. t-channel (tHq), c.,d. s-channel ($tH\bar{b}$), e.-i. W-associated.

762 ommiting the red line). The t-channel represents processes where an intermediate
 763 particle is emitted by one of the incoming particles and absorbed by the other. The
 764 s-channel represent processes where the two incoming particles merge into an inter-
 765 mediate particle which eventually will split into the particles in the final state. The
 766 third channel, u-channel, is similar to the t-channel but the two outgoing particles
 767 interchange their roles.

769 The th production where Higgs boson can be radiated either from the top quark or
 770 from the W boson is represented by the leading order Feynman diagrams in figure
 771 2.13. The cross section for the th process is calculated, as usual, summing over
 772 the contributions from the different feynman diagrams; therefore it depends on the
 773 interference between the contributions. In the SM, the interference for t-channel (tHq
 774 process) and W-associated (tHW process) production is destructive [46] resulting in
 775 the small cross sections presented in table 2.9.

| tH production channel | Cross section (fb) |
|---------------------------------------|-------------------------|
| t-channel ($pp \rightarrow tHq$) | $70.79^{+2.99}_{-4.80}$ |
| W-associated ($pp \rightarrow tHW$) | $15.61^{+0.83}_{-1.04}$ |
| s-channel($pp \rightarrow tHb$) | $2.87^{+0.09}_{-0.08}$ |

Table 2.9: Predicted SM cross sections for tH production at $\sqrt{s} = 13$ TeV [51, 52].

776

777 While the s-channel contribution can be neglected, it will be shown that a deviation
 778 from the SM destructive interference would result in an enhancement of the th cross
 779 section compared to that in SM, which could be used to get information about the
 780 sign of the Higgs-top coupling [48, 49]. In order to describe th production processes,
 781 Feynman diagram 2.13b will be considered; there, the W boson is radiated by a
 782 quark in the proton and eventually it will interact with the b quark. In the high
 783 energy regime, the effective W approximation [53] allows to describe the process as
 784 the emmision of an approximately on-shell W and its hard scattering with the b
 785 quark; i.e. $Wb \rightarrow th$. The scattering amplitude for the process is given by

$$\mathcal{A} = \frac{g}{\sqrt{2}} \left[(C_t - C_V) \frac{m_t \sqrt{s}}{m_W v} A \left(\frac{t}{s}, \varphi; \xi_t, \xi_b \right) + \left(C_V \frac{2m_W}{v} \frac{s}{t} + (2C_t - C_V) \frac{m_t^2}{m_W v} \right) B \left(\frac{t}{s}, \varphi; \xi_t, \xi_b \right) \right], \quad (2.57)$$

where $C_V \equiv g_{HVV}/g_{HVV}^{SM}$ and $C_t \equiv g_{Ht}/g_{Ht}^{SM} = y_t/y_t^{SM}$ are scaling factors that quantify possible deviations of the couplings, Higgs-Vector boson (H-W) and Higgs-top (H-t) respectively, from the SM couplings; $s = (p_W + p_b)^2$, $t = (p_W - p_H)^2$, φ is the Higgs azimuthal angle around the z axis taken parallel to the direction of motion of the incoming W; A and B are functions describing the weak interaction in terms of the chiral states of the quarks b and t. Terms that vanish in the high energy limit have been neglected as well as the Higgs and b quark masses⁹.
 The scattering amplitude grows with energy like \sqrt{s} for $C_V \neq C_t$, in contrast to the SM ($C_t = C_V = 1$) where the first term in 2.57 cancels out and the amplitude is constant for large s; therefore, a deviation from the SM predictions represent an enhancement in the tHq cross section. In particular, for a SM H-W coupling and a H-t coupling of inverted sign with respect to the SM ($C_V = -C_t = 1$) the tHq cross section is enhanced by a factor greater 10 as seen in the figure 2.14 taken from reference [48]; reference [54] have reported similar enhancement results.
 A similar analysis is valid for the W-associated channel but, in that case, the interference is more complicated since there are more than two contributions and an additional interference with the production of Higgs boson and a top pair process($t\bar{t}H$).
 The calculations are made using the so-called Diagram Removal (DR) technique where interfering diagrams are removed (or added) from the calculations in order to evaluate the impact of the removed contributions. DR1 was defined to neglect $t\bar{t}H$ interference while DR2 was defined to take $t\bar{t}H$ interference into account [55]. As shown in figure 2.15, the tHW cross section is enhanced from about 15 fb (SM: $\kappa_{Htt} = 1$) to about 150 fb ($\kappa_{Htt} = -1$). Differences between curves for DR1 and DR2 help to gauge the impact of the interference with $t\bar{t}H$.

⁹ A detailed explanation of the structure and approximations used to derive \mathcal{A} can be found in reference [48]

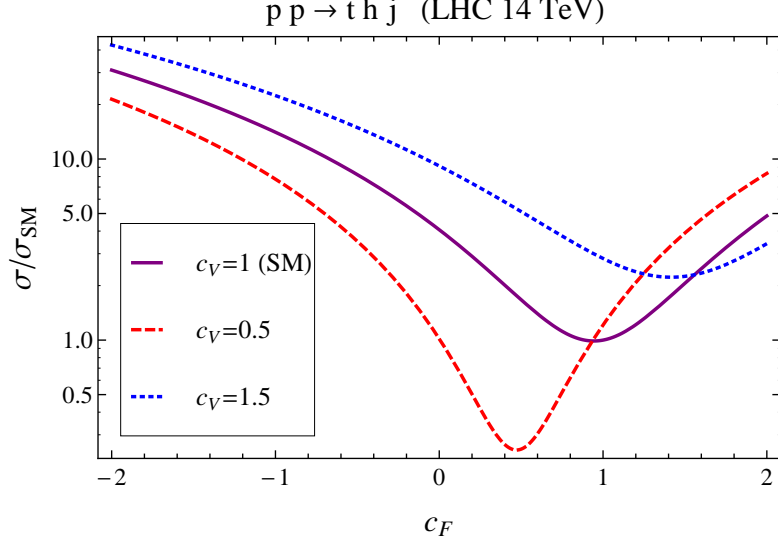


Figure 2.14: Cross section for tHq process as a function of C_t , normalized to the SM, for three values of C_V . In the plot C_f refers to the Higgs-fermion coupling which is dominated by the H-t coupling C_t . Solid, dashed and dotted lines correspond to $C_V = 1, 0.5, 1.5$ respectively. Note that for the SM ($C_V = C_t = 1$), the destructive effect of the interference is maximal.

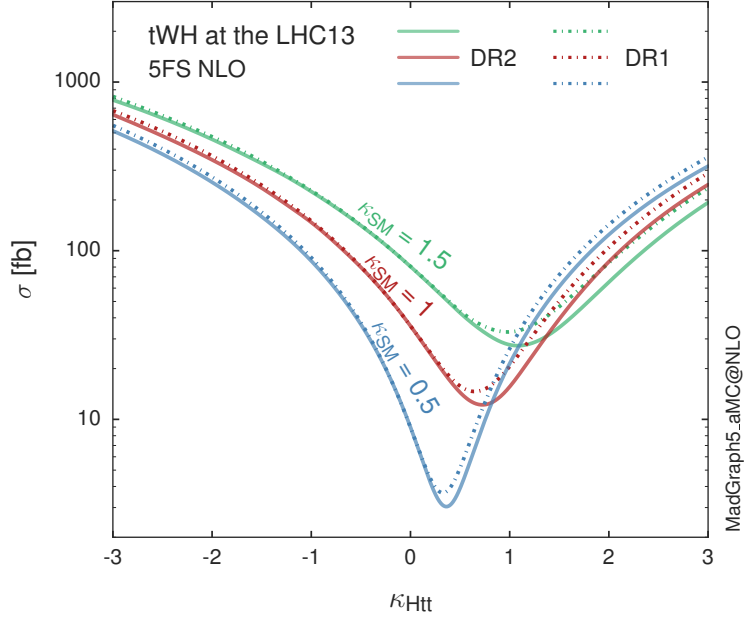


Figure 2.15: Cross section for tHW process as a function of κ_{Htt} , for three values of κ_{SM} at $\sqrt{s} = 13$ TeV. $\kappa_{Htt}^2 = \sigma_{Htt}/\sigma_{Htt}^{SM}$ is a simple rescaling of the SM Higgs interactions.

810 Results of the calculations of the tHq and tHW cross sections at $\sqrt{s} = 13$ TeV can be
 811 found in reference [56] and a summary of the results is presented in table 2.10.

| | \sqrt{s} TeV | $C_t = 1$ | $C_t = -1$ |
|--|----------------|-------------------------------|-----------------------------|
| $\sigma^{LO}(tHq)(\text{fb})$ [48] | 8 | ≈ 17.4 | ≈ 252.7 |
| | 14 | ≈ 80.4 | ≈ 1042 |
| $\sigma^{NLO}(tHq)(\text{fb})$ [48] | 8 | $18.28^{+0.42}_{-0.38}$ | $233.8^{+4.6}_{-0.0}$ |
| | 14 | $88.2^{+1.7}_{-0.0}$ | $982.8^{+28}_{-0.0}$ |
| $\sigma^{LO}(tHq)(\text{fb})$ [54] | 14 | ≈ 71.8 | ≈ 893 |
| $\sigma^{LO}(tHW)(\text{fb})$ [54] | 14 | ≈ 16.0 | ≈ 139 |
| $\sigma^{NLO}(tHq)(\text{fb})$ [56] | 8 | $18.69^{+8.62\%}_{-17.13\%}$ | - |
| | 13 | $74.25^{+7.48\%}_{-15.35\%}$ | $848^{+7.37\%}_{-13.70\%}$ |
| | 14 | $90.10^{+7.34\%}_{-15.13\%}$ | $1011^{+7.24\%}_{-13.39\%}$ |
| $\sigma^{LO}(tHW)(\text{fb})$ [55] | 13 | $15.77^{+15.91\%}_{-15.76\%}$ | - |
| $\sigma^{NLO}DR1(tHW)(\text{fb})$ [55] | 13 | $21.72^{+6.52\%}_{-5.24\%}$ | ≈ 150 |
| $\sigma^{NLO}DR2(tHW)(\text{fb})$ [55] | 13 | $16.28^{+7.34\%}_{-15.13\%}$ | ≈ 150 |

Table 2.10: Predicted enhancement of the tHq and tHW cross sections at LHC for $C_V = 1$ and $C_t = \pm 1$ at LO and NLO; the cross section enhancement of more than a factor of 10 is due to the flippling in the sign of the H-t coupling with respect to the SM one.

812

813 2.5 The CP-mixing in tH processes

814 In addition to the sensitivity to sign of the H-t coupling, tHq and tHW processes have
 815 been proposed as a tool to investigate the possibility of a H-t coupling that does not
 816 conserve CP [50, 55, 57]. Current experimental results are consistent with SM H-V
 817 and H-t couplings; however, negative H-t coupling is not excluded completely [60].

818

819 In this thesis, the sensitivity of th processes to CP-mixing is also studied in the
 820 effective field theory framework and based in references [50, 55]; a generic particle
 821 (X_0) of spin-0 and a general CP violating interaction with the top quark, can couples

822 to scalar and pseudoscalar fermionic densities. The H-W interaction is assumed to
 823 be SM-like. The Lagrangian modeling the H-t interaction is given by

$$\mathcal{L}_0^t = -\bar{\psi}_t (c_\alpha \kappa_{Htt} g_{Htt} + i s_\alpha \kappa_{Att} g_{Att} \gamma_5) \psi_t X_0, \quad (2.58)$$

824 where α is the CP-mixing phase, $c_\alpha \equiv \cos \alpha$ and $s_\alpha \equiv \sin \alpha$, κ_{Htt} and κ_{Att} are real
 825 dimensionless rescaling parameters¹⁰, $g_{Htt} = g_{Att} = m_t/v = y_t/\sqrt{2}$ and $v \sim 246$ GeV
 826 is the Higgs vacuum expectation value. In this parametrization, it is easy to recover
 827 three special cases

- 828 • CP-even coupling $\rightarrow \alpha = 0^\circ$
- 829 • CP-odd coupling $\rightarrow \alpha = 90^\circ$
- 830 • SM coupling $\rightarrow \alpha = 0^\circ$ and $\kappa_{Htt} = 1$

831 The loop induced X_0 coupling to gluons can also be described in terms of the
 832 parametrization above, according to

$$\mathcal{L}_0^g = -\frac{1}{4} (c_\alpha \kappa_{Hgg} g_{Hgg} G_{\mu\nu}^a G^{a,\mu\nu} + s_\alpha \kappa_{Agg} g_{Agg} G_{\mu\nu}^a \tilde{G}^{a,\mu\nu}) X_0. \quad (2.59)$$

833 where $g_{Hgg} = -\alpha_s/3\pi v$ and $g_{Agg} = \alpha_s/2\pi v$. Under the assumption that the top quark
 834 dominates the gluon-fusion process at LHC energies, $\kappa_{Hgg} \rightarrow \kappa_{Htt}$ and $\kappa_{Agg} \rightarrow \kappa_{Att}$,
 835 so that the ratio between the gluon-gluon fusion cross section for X_0 and for the SM
 836 Higgs prediction can be written as

$$\frac{\sigma_{NLO}^{gg \rightarrow X_0}}{\sigma_{NLO,SM}^{gg \rightarrow H}} = c_\alpha^2 \kappa_{Htt}^2 + s_\alpha^2 \left(\kappa_{Att} \frac{g_{Agg}}{g_{Hgg}} \right)^2. \quad (2.60)$$

837 If the rescaling parameters are set to

¹⁰ analog to C_t and C_V

$$\kappa_{Htt} = 1, \quad \kappa_{Att} = \left| \frac{g_{Hgg}}{g_{Agg}} \right| = \frac{2}{3}. \quad (2.61)$$

the gluon-fusion SM cross section is reproduced for every value of the CP-mixing angle α ; therefore, by imposing that condition to the Lagrangian density 2.58, the CP-mixing angle is not constrained by current data. Figure 2.16 shows the NLO cross sections for t-channel tX_0 (blue) and $t\bar{t}X_0$ (red) associated production processes as a function of the CP-mixing angle α . X_0 is a generic spin-0 particle with top quark CP-violating coupling. Rescaling factors κ_{Htt} and κ_{Att} have been set to reproduce the SM gluon-fusion cross sections.

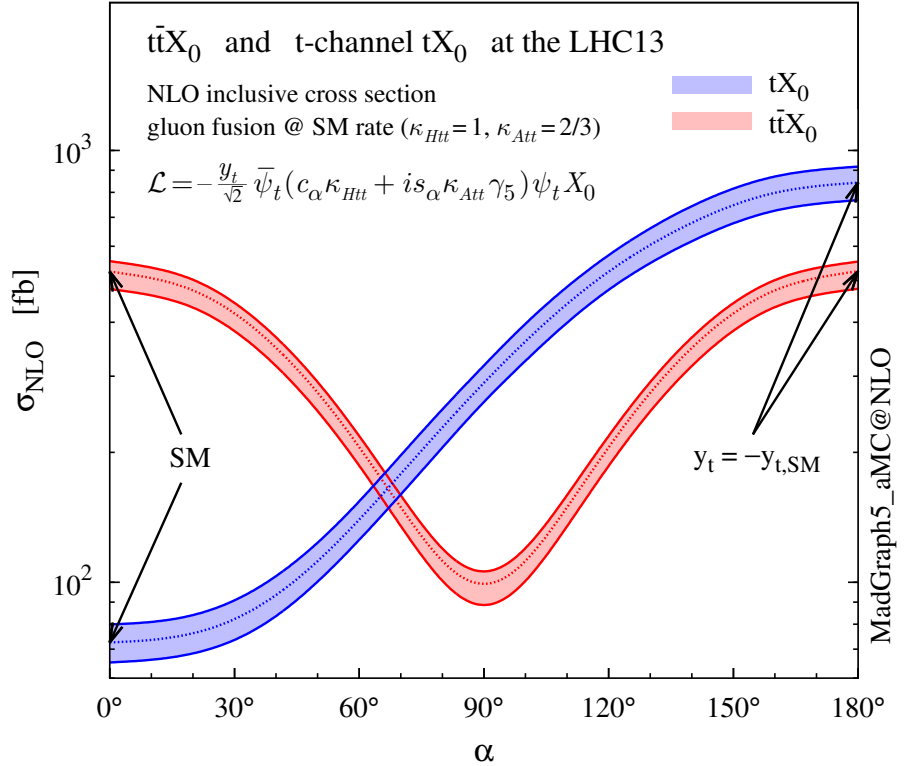


Figure 2.16: NLO cross sections for t-channel tX_0 (blue) and $t\bar{t}X_0$ (red) associated production processes as a function of the CP-mixing angle α . X_0 is a generic spin-0 particle with top quark CP-violating coupling [50].

845 It is interesting to notice that the tX_0 cross section is enhanced, by a factor of
 846 about 10, when a continuous rotation in the scalar-pseudoscalar plane is applied; this
 847 enhancement is similar to the enhancement produced when the H-t coupling is flipped
 848 in sign with respect to the SM ($y_t = -y_{t,SM}$ in the plot), as showed in section 2.4. In
 849 contrast, the degeneracy in the $t\bar{t}X_0$ cross section is still present given that it depends
 850 quadratically on the H-t coupling, but more interesting is to notice that $t\bar{t}X_0$ cross
 section is exceeded by tX_0 cross section after $\alpha \sim 60^\circ$.

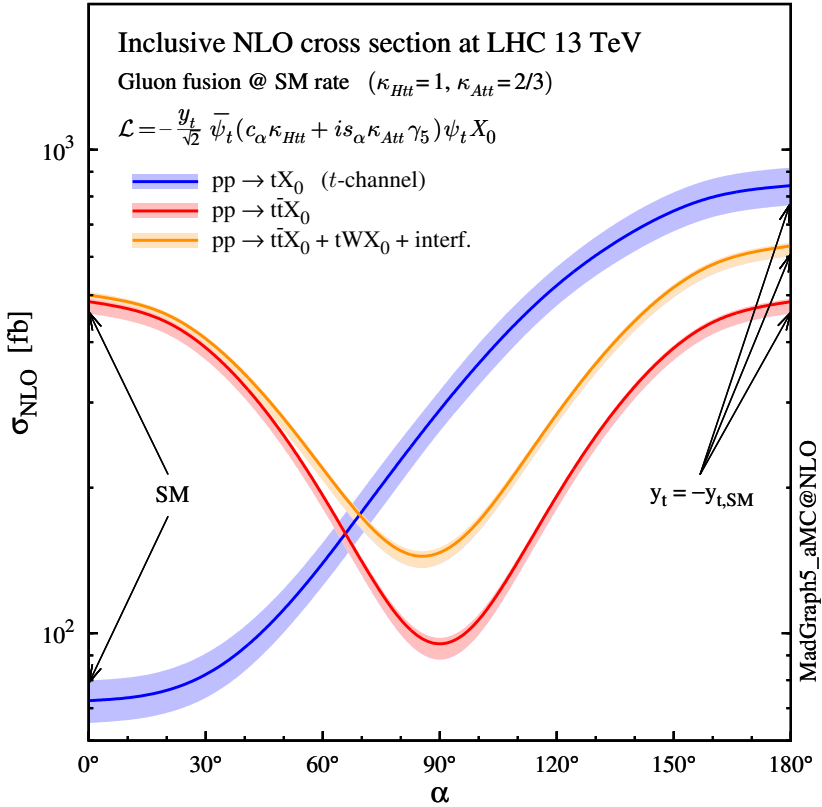


Figure 2.17: NLO cross sections for t-channel tX_0 (blue), $t\bar{t}X_0$ (red) associated production processes and combined $tWX_0 + t\bar{t}X_0$ (including interference) production as a function of the CP-mixing angle α [50].

851

852 A similar parametrization can be used to investigate the tHW process sensitivity to
 853 CP-violating H-t coupling. As said in 2.4, the interference in the W-associated channel
 854 is more complicated because there are more than two contributions and also there is

855 interference with the $t\bar{t}H$ production process.

856 Figure 2.17 shows the NLO cross sections for t-channel tX_0 (blue), $t\bar{t}X_0$ (red) asso-
857 ciated production and for the combined $tWX_0 + t\bar{t}X_0 +$ interference (orange) as a
858 function of the CP-mixing angle. It is clear that the effect of the interference in the
859 combined case is the lifting of the degeneracy present in the $t\bar{t}X_0$ production. The
860 constructive interference enhance the cross section from about 500 fb at SM ($\alpha = 0$)
861 to about 600 fb ($\alpha = 180^\circ \rightarrow y_t = -y_{t,SM}$).

862 An analysis combining tHq and tHW proceses will be made in this thesis taking
863 advantage of the sensitivity improvement.

⁸⁶⁴ **Chapter 3**

⁸⁶⁵ **The CMS experiment at the LHC**

⁸⁶⁶ **3.1 Introduction**

⁸⁶⁷ Located in the Swiss-French border, the European Council for Nuclear Research
⁸⁶⁸ (CERN) is the largest scientific organization leading the particle physics research.
⁸⁶⁹ About 13000 people in a broad range of fields including users, students, scientists,
⁸⁷⁰ engineers among others, contribute to the data taking and analysis, with the goal
⁸⁷¹ of unveiling the secrets of the nature and revealing the fundamental structure of the
⁸⁷² universe. CERN is also the home of the Large Hadron Collider (LHC), the largest
⁸⁷³ circular particle accelerator around the world, where protons (or heavy ions) traveling
⁸⁷⁴ close to the speed of light, are made to collide. These collisions open a window to
⁸⁷⁵ investigate how particles (and their constituents if they are composite) interact with
⁸⁷⁶ each other, providing clues about the laws of the nature.

⁸⁷⁷ LHC can run in three modes depending on the particles being accelerated

- ⁸⁷⁸ • Proton-Proton collisions (pp) multiple physics experiments .
⁸⁷⁹ • Lead-Lead collisions (Pb-Pb) Heavy ion experiments.

- 880 • Proton-Lead collisions (p-Pb).

881 Figure 3.1 show an overview of the CERN accelerating complex. There are several
 882 accelerating stages before the injection to the LHC ring. In the pp mode, after
 883 removing the electrons from hydrogen atoms in a bottle, protons are accelerated
 884 in the LINAC2 to 50 MeV and then injected into the proton synchrotron booster
 885 (BOOSTER) to reach 1.4 GeV in energy. The next boost is provided at the proton
 886 synchrotron (PS) up to 26 GeV, followed by the injection into the super proton
 887 synchrotron (SPS) where protons are accelerated to 450 GeV. Finally, protons are
 888 injected into the LHC where they are accelerated to the target energy of 6.5 TeV. In
 889 the Pb-Pb mode, the Lead ions are first accelerated in the LINAC3 and then passed as
 890 long pulses to the Low energy ion ring (LEIR) to be converted into short and dense
 891 bunches, each containing 7×10^7 lead ions. LEIR accelerate the bunches from 4.2
 892 MeV to 72 MeV. The ions are then passed to the PS to follow the rest of acceleration
 893 process up to 2.8TeV/n en the LHC ring.

894 **3.2 The LHC**

895 The LHC is a 27 km ring composed of superconducting magnets and accelerating
 896 structures (among other components) which boost the particles traveling inside it.
 897 It is installed in the same tunnel where the large Electron-Positron (LEP) collider
 898 was located, taking advantage of the existing infraestructure as shown in Figure 3.2.
 899 Two particle beams travel counter-rotating in two separated beam pipes kept at ultra
 900 high vacuum. In 2008, the first set of collisions involved protons with center-of-mass
 901 energy of 7 TeV after which the energy was increased to 8 TeV in 2012 and to 13 TeV
 902 in 2015.

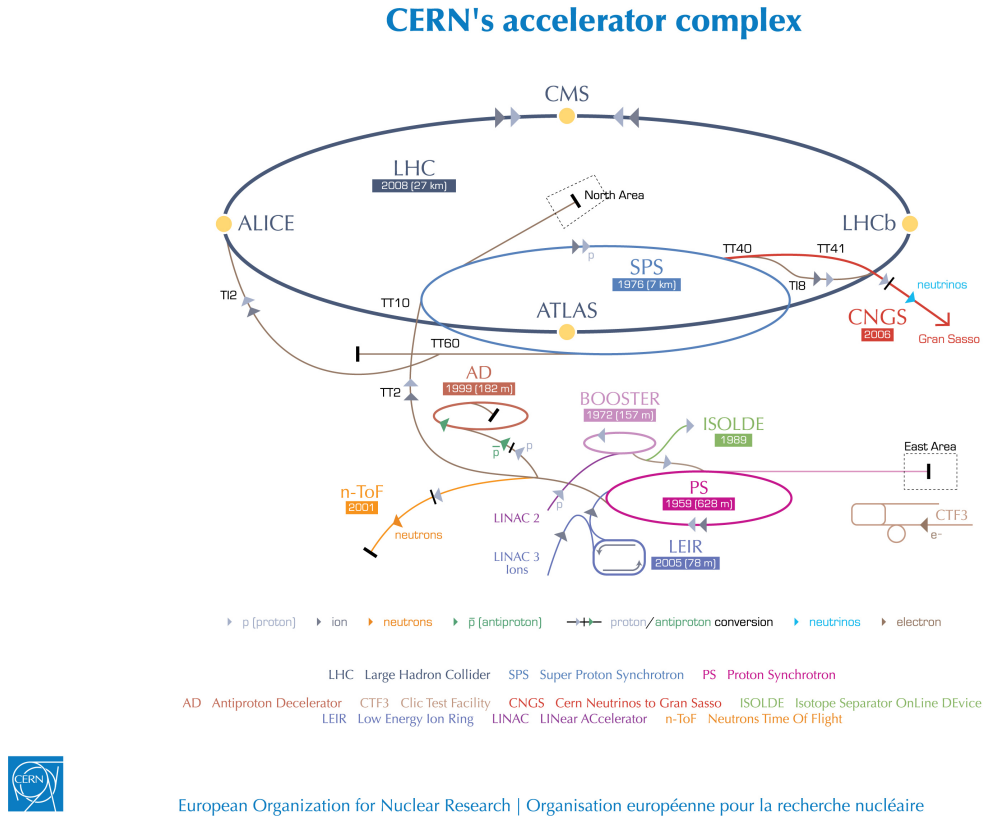
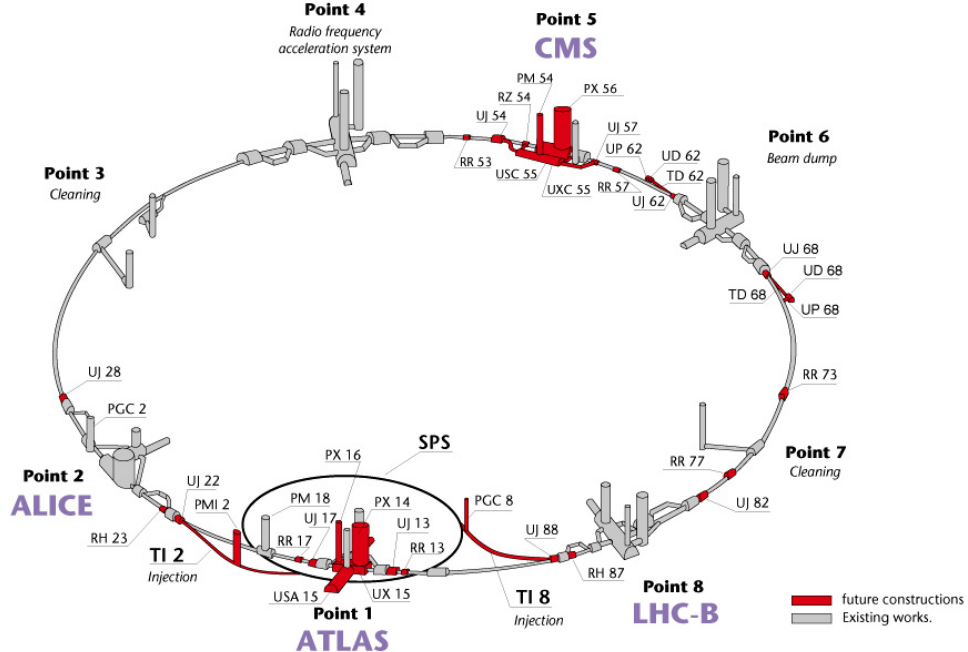


Figure 3.1: ref. C.Lefevre, “The CERN accelerator complex,” (2008). CERN-DI-0812015.

903 In order to keep the protons in the circular trajectory carrying that amount of
 904 energy, strong magnetic fields are needed, bringing the superconductivity into scene.
 905 The superconducting dipole magnets used in LHC are made of a NbTi alloy, capable
 906 of transporting currents of about 12000 A when cooled at a temperature below 2K by
 907 using liquid helium; that current generates a magnetic fields of 8.3 T. Figure 3.3 shows
 908 the transverse view of the LHC dipole magnets. Additionally, quadrupole magnets
 909 are used to focus the beam and some other magnetic multipoles are used to correct
 910 effects generated by the interaction among protons in the beam as well as interactions
 911 within the beam pipe.
 912 Regarding to the longitudinal acceleration of the protons, a system of 16 radio-
 913 frecuency cavities (RF) (8 per beam) is used to accelerate protons. Inside the cavities,

Layout of the LEP tunnel including future LHC infrastructures.



CERN AC _ hf238 _ V02/02/98

Figure 3.2: ref. J.-L. Caron , “Layout of the LEP tunnel including future LHC infrastructures.. L’ensemble du tunnel LEP avec les futures infrastructures LHC.”, <https://cds.cern.ch/record/841542> (Nov, 1993). AC Collection. Legacy of AC. Pictures from 1992 to 2002..

914 the electromagnetic waves become resonant transferring the maximum energy to the
 915 particle flight through it. Cavities are cooled at 4.5 K. On LHC the RF oscillation
 916 frecuency is 400MHz and the protons are carefully timed so additionally to the ac-
 917 celeration effect the bunch structure of the beam is preserved. The Beam is made
 918 of 2808 “bunches” which are packages of 1.15×10^{11} protons ???. If LHC is at full
 919 energy, protons with the right energy does not feel any accelerating force but those
 920 with a different energy will be accelerated or decelerated to keep them in the bunch.
 921 The paths followed by particles during the acceleration process are shown in Figure
 922 3.1.

LHC DIPOLE : STANDARD CROSS-SECTION

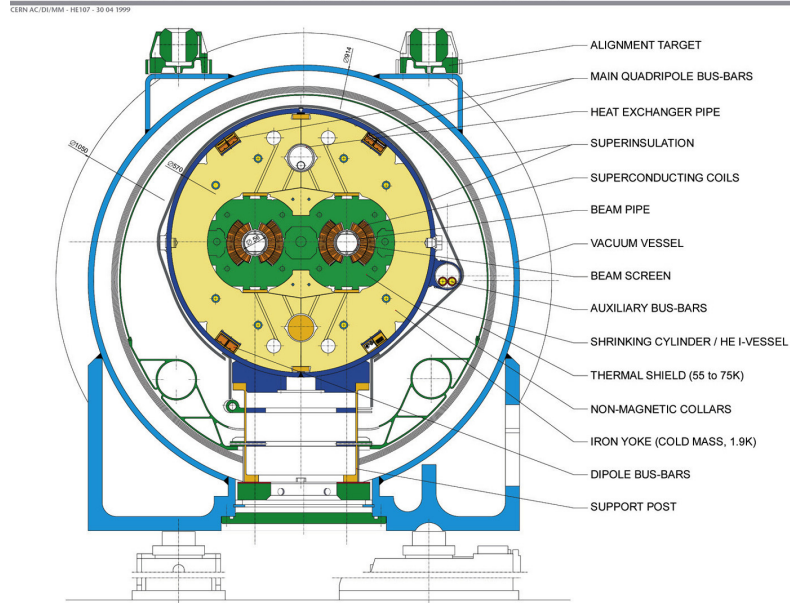


Figure 3.3: ref. ACTeam, “Diagram of an LHC dipole magnet. Schéma d’un aimant dipôle du LHC,” (1999). CERN-DI-9906025.

923 Once the beams reach the desired energy, they are brought to cross each other
 924 producing proton-proton collisions. The bunch crossing happens in precise places
 925 where the LHC experiments are located. As seen in Figure 3.2, it was needed to
 926 build the caverns for CMS and ATLAS as well as some additional facilities, but
 927 most of the initial LEP infrastructure has been used to allocate additional collision
 928 points. The highest luminosity is delivered at the CMS (point 5) and ATLAS (point
 929 1) experiments, which are general purpose experiments, enabled to explore physics
 930 in any of the collision modes. LHCb (point 8) experiment is optimized to explore
 931 B-physics, while ALICE (point 2) is optimized for heavy ion collisions researches;
 932 TOTEM (point 5) and LHCf (point 1) are dedicated to forward physics studies and
 933 MoEDAL (point 8) is intended for monopoles or massive pseudo stable particles
 934 studies.

935 3.3 The CMS experiment

936 The Compact Muon Solenoid (CMS) is a general purpose detector designed to conduct
937 research in a wide range of physics from standard model to new physics like extra
938 dimensions and dark matter. Located at the point 5 in the LHC layout as shown in
939 Figure 3.2, CMS is composed by several detection systems distributed in a cylindrical
940 structure where the main feature is a solenoid magnet made of superconducting cable
941 capable to generate a 3.8 T magnetic field. In total, CMS weight about 14000 tons
942 in a very compact 21.6 m long and 14.6 m diameter cylinder (include areference for
943 CMS TDR). It was built in 15 separated sections at the ground level and lowered
944 to the cavern individually to be assembled. Figure 3.4 show the layout of the CMS
945 detector (CMS TDR).

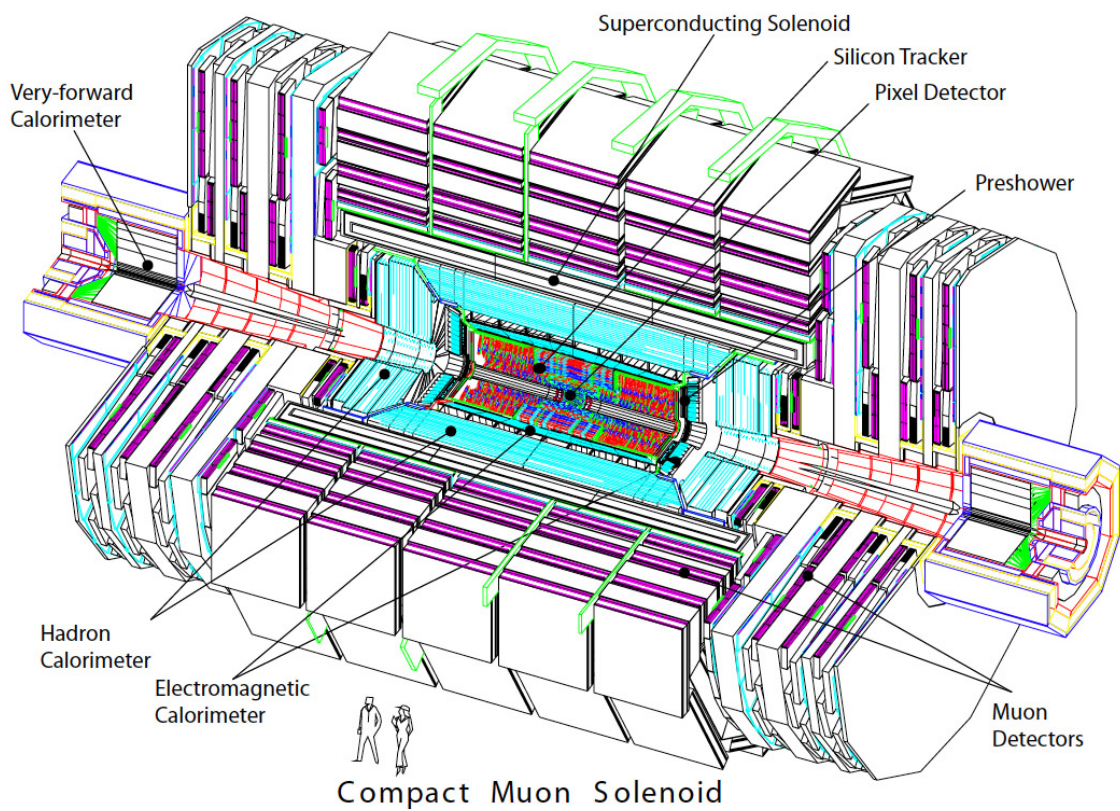


Figure 3.4: ref: CMS Collaboration, “Detector Drawings”, CMS-PHO-GEN-2012-002, <http://cds.cern.ch/record/1433717>, 2012.

⁹⁴⁶ Chapter 4

⁹⁴⁷ **Search for production of a Higgs**
⁹⁴⁸ **boson and a single top quark in**
⁹⁴⁹ **multilepton final states in pp**
⁹⁵⁰ **collisions at $\sqrt{s} = 13$ TeV**

⁹⁵¹ 4.1 Introduction

⁹⁵² Dont forget to mention previous constrains to ct check reference ?? and references
⁹⁵³ <https://link.springer.com/content/pdf/10.1007%2FJHEP01>
⁹⁵⁴ A. Azatov, R. Contino and J. Galloway, â€œModel-Independent Bounds on a
⁹⁵⁵ Light Higgs,â€ JHEP 1204 (2012) 127 [arXiv:1202.3415 [hep-ph]].
⁹⁵⁶ J. R. Espinosa, C. Grojean, M. Muhlleitner and M. Trott, â€œFingerprinting
⁹⁵⁷ Higgs Suspects at the LHC,â€ JHEP 1205 (2012) 097 [arXiv:1202.3697 [hep-ph]].
⁹⁵⁸ This chapter present the search for the associated production of a Higgs boson and
⁹⁵⁹ a single top quark events with three leptons in the final state, targeting Higgs decay

960 modes to WW , ZZ , and $\tau\tau$. The analysis uses the 13 TeV dataset produced in 2016,
 961 corresponding to an integrated luminosity of 35.9fb^{-1} . It is based on and expands
 962 previous analyses at 8 TeV [61, 62] and searches for associated production of $t\bar{t}$ and
 963 Higgs in the same channel [63], and complements searches in other decay channels
 964 targeting $H \rightarrow b\bar{b}$ [64].

965 As showed in section 2.4, the cross section of the associated production of a Higgs
 966 boson and a single top quark (tHq) process is driven by a destructive interference of
 967 two contributions (see Figure 4.1), where the Higgs couples to either the W boson or
 968 the top quark. Any deviation from the standard model (SM) in the Higgs coupling
 969 structure could therefore lead to a large enhancement of the cross section, making
 970 this analysis sensitive to such deviations. A second process, where the Higgs and
 971 top quark are accompanied by a W boson (tHW) has similar behavior, albeit with a
 972 weaker interference pattern.

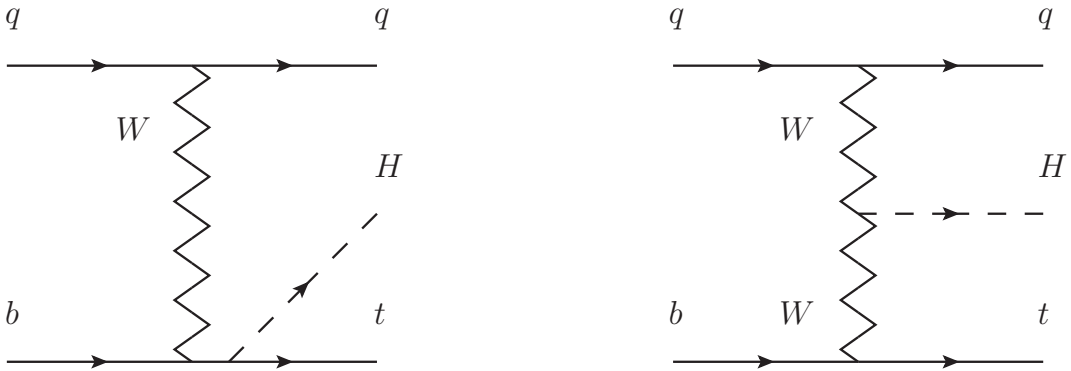


Figure 4.1: The two leading-order diagrams of tHq production.

973 We selects events with three leptons and a b tagged jet in the final state. The tHq
 974 signal contribution is then determined in a fit of the observed data to two multivariate
 975 classifier outputs, each trained to discriminate against one of the two dominant back-
 976 grounds of events with non-prompt leptons from $t\bar{t}$ and of associated production of $t\bar{t}$

977 and vector bosons ($t\bar{t}W$, $t\bar{t}Z$). The fit result is then used to set an upper limit on the
 978 combined $t\bar{t}H$, tHq and tHW production cross section, as a function of the relative
 979 coupling strengths of Higgs and top quark and Higgs and W boson, respectively.

980 4.2 Data and MC Samples

981 The data considered in this analysis were collected by the CMS experiment dur-
 982 ing 2016 and correspond to a total integrated luminosity of 35.9fb^{-1} . Only periods
 983 when the CMS magnet was on were considered when selecting the data samples, that
 984 corresponds to the 23 Sep 2016 (Run B to G) and PromptReco (Run H) versions
 985 of the datasets. The MC samples used in this analysis correspond to the RunI-
 986 ISummer16MiniAODv2 campaign produced with CMSSW 80X. The two signal sam-
 987 ples (for tHq and tHW) were produced with MG5_aMC@NLO (version 5.222), in
 988 leading-order mode, and are normalized to next-to-leading-order cross sections,
 989 see Tab. 4.1. Each sample is generated with a set of event weights corresponding to
 990 different values of κ_t and κ_V couplings as shown in Tab. 4.2.

991 4.2.1 Full 2016 dataset and MC samples

| Sample | σ [pb] | BF |
|---|---------------|-------|
| /THQ_Hincl_13TeV-madgraph-pythia8_TuneCUETP8M1/ | 0.7927 | 0.324 |
| /THW_Hincl_13TeV-madgraph-pythia8_TuneCUETP8M1/ | 0.1472 | 1.0 |

Table 4.1: Signal samples and their cross section and branching fraction used in this analysis. See Ref. [65] for more details.

992 Different MC generators were used to generate the background processes. The
 993 dominant sources ($t\bar{t}$, $t\bar{t}W$, $t\bar{t}Z$, $t\bar{t}H$) were produced using AMC@NLO interfaced
 994 to PYTHIA8, and are scaled to NLO cross sections. Other processes are simulated

| | | <i>tHq</i> | | <i>tHW</i> | | |
|------------|------------|----------------|--------------------|----------------|--------------------|--------------------|
| κ_V | κ_t | sum of weights | cross section [pb] | sum of weights | cross section [pb] | LHE weights |
| 1.0 | -3.0 | 35.700022 | 2.991 | 11.030445 | 0.6409 | LHEweight_wgt[446] |
| 1.0 | -2.0 | 20.124298 | 1.706 | 5.967205 | 0.3458 | LHEweight_wgt[447] |
| 1.0 | -1.5 | 14.043198 | 1.205 | 4.029093 | 0.2353 | LHEweight_wgt[448] |
| 1.0 | -1.25 | 11.429338 | 0.9869 | 3.208415 | 0.1876 | LHEweight_wgt[449] |
| 1.0 | -1.0 | | 0.7927 | | 0.1472 | |
| 1.0 | -0.75 | 7.054998 | 0.6212 | 1.863811 | 0.1102 | LHEweight_wgt[450] |
| 1.0 | -0.5 | 5.294518 | 0.4723 | 1.339886 | 0.07979 | LHEweight_wgt[451] |
| 1.0 | -0.25 | 3.818499 | 0.3505 | 0.914880 | 0.05518 | LHEweight_wgt[452] |
| 1.0 | 0.0 | 2.627360 | 0.2482 | 0.588902 | 0.03881 | LHEweight_wgt[453] |
| 1.0 | 0.25 | 1.719841 | 0.1694 | 0.361621 | 0.02226 | LHEweight_wgt[454] |
| 1.0 | 0.5 | 1.097202 | 0.1133 | 0.233368 | 0.01444 | LHEweight_wgt[455] |
| 1.0 | 0.75 | 0.759024 | 0.08059 | 0.204034 | 0.01222 | LHEweight_wgt[456] |
| 1.0 | 1.0 | 0.705305 | 0.07096 | 0.273617 | 0.01561 | LHEweight_wgt[457] |
| 1.0 | 1.25 | 0.936047 | 0.0839 | 0.442119 | 0.02481 | LHEweight_wgt[458] |
| 1.0 | 1.5 | 1.451249 | 0.1199 | 0.709538 | 0.03935 | LHEweight_wgt[459] |
| 1.0 | 2.0 | 3.335034 | 0.2602 | 1.541132 | 0.08605 | LHEweight_wgt[460] |
| 1.0 | 3.0 | 10.516125 | 0.8210 | 4.391335 | 0.2465 | LHEweight_wgt[461] |
| <hr/> | | | | | | |
| 1.5 | -3.0 | 45.281492 | 3.845 | 13.426212 | 0.7825 | LHEweight_wgt[462] |
| 1.5 | -2.0 | 27.606715 | 2.371 | 7.809713 | 0.4574 | LHEweight_wgt[463] |
| 1.5 | -1.5 | 20.476088 | 1.784 | 5.594971 | 0.3290 | LHEweight_wgt[464] |
| 1.5 | -1.25 | 17.337465 | 1.518 | 4.635978 | 0.2749 | LHEweight_wgt[465] |
| 1.5 | -1.0 | 14.483302 | 1.287 | 3.775902 | 0.2244 | LHEweight_wgt[466] |
| 1.5 | -0.75 | 11.913599 | 1.067 | 3.014744 | 0.1799 | LHEweight_wgt[467] |
| 1.5 | -0.5 | 9.628357 | 0.874 | 2.352505 | 0.1410 | LHEweight_wgt[468] |
| 1.5 | -0.25 | 7.627574 | 0.702 | 1.789184 | 0.1081 | LHEweight_wgt[469] |
| 1.5 | 0.0 | 5.911882 | 0.5577 | 1.324946 | 0.08056 | LHEweight_wgt[470] |
| 1.5 | 0.25 | 4.479390 | 0.4365 | 0.959295 | 0.05893 | LHEweight_wgt[471] |
| 1.5 | 0.5 | 3.331988 | 0.3343 | 0.692727 | 0.04277 | LHEweight_wgt[472] |
| 1.5 | 0.75 | 2.469046 | 0.2558 | 0.525078 | 0.03263 | LHEweight_wgt[473] |
| 1.5 | 1.0 | 1.890565 | 0.2003 | 0.456347 | 0.02768 | LHEweight_wgt[474] |
| 1.5 | 1.25 | 1.596544 | 0.1689 | 0.486534 | 0.02864 | LHEweight_wgt[475] |
| 1.5 | 1.5 | 1.586983 | 0.1594 | 0.615638 | 0.03509 | LHEweight_wgt[476] |
| 1.5 | 2.0 | 2.421241 | 0.2105 | 1.170602 | 0.06515 | LHEweight_wgt[477] |
| 1.5 | 3.0 | 7.503280 | 0.5889 | 3.467546 | 0.1930 | LHEweight_wgt[478] |
| <hr/> | | | | | | |
| 0.5 | -3.0 | 27.432685 | 2.260 | 8.929074 | 0.5136 | LHEweight_wgt[479] |
| 0.5 | -2.0 | 13.956013 | 1.160 | 4.419093 | 0.2547 | LHEweight_wgt[480] |
| 0.5 | -1.5 | 8.924438 | 0.7478 | 2.757611 | 0.1591 | LHEweight_wgt[481] |
| 0.5 | -1.25 | 6.835341 | 0.5726 | 2.075247 | 0.1204 | LHEweight_wgt[482] |
| 0.5 | -1.0 | 5.030704 | 0.4273 | 1.491801 | 0.08696 | LHEweight_wgt[483] |
| 0.5 | -0.75 | 3.510528 | 0.2999 | 1.007273 | 0.05885 | LHEweight_wgt[484] |
| 0.5 | -0.5 | 2.274811 | 0.1982 | 0.621663 | 0.03658 | LHEweight_wgt[485] |
| 0.5 | -0.25 | 1.323555 | 0.1189 | 0.334972 | 0.01996 | LHEweight_wgt[486] |
| 0.5 | 0.0 | 0.656969 | 0.06223 | 0.147253 | 0.008986 | LHEweight_wgt[487] |
| 0.5 | 0.25 | 0.274423 | 0.02830 | 0.058342 | 0.003608 | LHEweight_wgt[488] |
| 0.5 | 0.5 | 0.176548 | 0.01778 | 0.068404 | 0.003902 | LHEweight_wgt[489] |
| 0.5 | 0.75 | 0.363132 | 0.03008 | 0.177385 | 0.009854 | LHEweight_wgt[490] |
| 0.5 | 1.0 | 0.834177 | 0.06550 | 0.385283 | 0.02145 | LHEweight_wgt[491] |
| 0.5 | 1.25 | 1.589682 | 0.1241 | 0.692099 | 0.03848 | LHEweight_wgt[492] |
| 0.5 | 1.5 | 2.629647 | 0.2047 | 1.097834 | 0.06136 | LHEweight_wgt[493] |
| 0.5 | 2.0 | 5.562958 | 0.4358 | 2.206057 | 0.1246 | LHEweight_wgt[494] |
| 0.5 | 3.0 | 14.843102 | 1.177 | 5.609519 | 0.3172 | LHEweight_wgt[495] |

Table 4.2: κ_V and κ_t combinations generated for the two signal samples and their NLO cross sections. The *tHq* cross section is multiplied by the branching fraction of the enforced leptonic decay of the top quark (0.324). See also Ref. [65].

| Sample | σ [pb] |
|--|------------------|
| TTWJetsToLNu_TuneCUETP8M1_13TeV-amcatnloFXFX-madspin-pythia8 | 0.2043 |
| TTZToLLNuNu_M-10_TuneCUETP8M1_13TeV-amcatnlo-pythia8 | 0.2529 |
| ttHJetToNonbb_M125_13TeV_amcatnloFXFX_madspin_pythia8_mWCutfix /store/cmst3/group/susy/gpetrucc/13TeV/u/TTLL_m1to10_LO_NoMS_for76X/ | 0.2151 0.0283 |
| WGToLNug_TuneCUETP8M1_13TeV-madgraphMLM-pythia8 | 585.8 |
| ZGTo2LG_TuneCUETP8M1_13TeV-amcatnloFXFX-pythia8 | 131.3 |
| TGJets_TuneCUETP8M1_13TeV_amcatnlo_madspin_pythia8 | 2.967 |
| TGJets_TuneCUETP8M1_13TeV_amcatnlo_madspin_pythia8 | 2.967 |
| TTGJets_TuneCUETP8M1_13TeV-amcatnloFXFX-madspin-pythia8 | 3.697 |
| WpWpJJ_EWK-QCD_TuneCUETP8M1_13TeV-madgraph-pythia8 | 0.03711 |
| ZZZ_TuneCUETP8M1_13TeV-amcatnlo-pythia8 | 0.01398 |
| WWZ_TuneCUETP8M1_13TeV-amcatnlo-pythia8 | 0.1651 |
| WZZ_TuneCUETP8M1_13TeV-amcatnlo-pythia8 | 0.05565 |
| WW_DoubleScattering_13TeV-pythia8 | 1.64 |
| tZq_1l_4f_13TeV-amcatnlo-pythia8_TuneCUETP8M1 | 0.0758 |
| ST_tW1l_5f_L0_13TeV-MadGraph-pythia8 | 0.01123 |
| TTTT_TuneCUETP8M1_13TeV-amcatnlo-pythia8 | 0.009103 |
| WZTo3LNu_TuneCUETP8M1_13TeV-powheg-pythia8 | 4.4296 |
| ZZTo4L_13TeV_powheg_pythia8 | 1.256 |
| TTJets_SingleLeptFromTbar_TuneCUETP8M1_13TeV-madgraphMLM-pythia8 | 182.1754 |
| TTJets_SingleLeptFromT_TuneCUETP8M1_13TeV-madgraphMLM-pythia8 | 182.1754 |
| TTJets_DiLept_TuneCUETP8M1_13TeV-madgraphMLM-pythia8 | 87.3 |
| DYJetsToLL_M-10to50_TuneCUETP8M1_13TeV-amcatnloFXFX-pythia8 | 18610 |
| DYJetsToLL_M-50_TuneCUETP8M1_13TeV-madgraphMLM-pythia8 | 6024 |
| WJetsToLNu_TuneCUETP8M1_13TeV-amcatnloFXFX-pythia8 | 61526.7 |
| ST_tW_top_5f_inclusiveDecays_13TeV-powheg-pythia8_TuneCUETP8M1 | 35.6 |
| ST_tW_antitop_5f_inclusiveDecays_13TeV-powheg-pythia8_TuneCUETP8M1 | 35.6 |
| ST_t-channel_4f_leptonDecays_13TeV-amcatnlo-pythia8_TuneCUETP8M1 | 70.3144 |
| ST_t-channel_antitop_4f_leptonDecays_13TeV-powheg-pythia8_TuneCUETP8M1 | 26.2278 |
| ST_s-channel_4f_leptonDecays_13TeV-amcatnlo-pythia8_TuneCUETP8M1 | 3.68064 |
| WWTo2L2Nu_13TeV-powheg | 10.481 |

Table 4.3: List of background samples used in this analysis (CMSSW 80X). In the first section of the table are listed the samples of the processes for which we use the simulation to extract the final yields and shapes, in the second section the samples of the processes we will estimate from data. The MC simulation is used to design the data driven methods and derive the associated systematics.

| Sample | σ [pb] |
|---------------------------|---------------|
| ttWJets_13TeV_madgraphMLM | 0.6105 |
| ttZJets_13TeV_madgraphMLM | 0.5297/0.692 |

Table 4.4: Leading-order $t\bar{t}W$ and $t\bar{t}Z$ samples used in the signal BDT training.

995 using POWHEG interfaced to PYTHIA, or bare PYTHIA (see table 4.3 and [63]
996 for more details).

| |
|--|
| Three lepton and Four lepton |
| HLT_DiMu9_Ele9_CaloIdL_TrackIdL_v* |
| HLT_Mu8_DiEle12_CaloIdL_TrackIdL_v* |
| HLT_TripleMu_12_10_5_v* |
| HLT_Ele16_Ele12_Ele8_CaloIdL_TrackIdL_v* |
| HLT_Mu23_TrkIsoVVL_Ele8_CaloIdL_TrackIdL_IsoVL_v* |
| HLT_Mu23_TrkIsoVVL_Ele8_CaloIdL_TrackIdL_IsoVL_DZ_v* |
| HLT_Mu8_TrkIsoVVL_Ele23_CaloIdL_TrackIdL_IsoVL_v* |
| HLT_Mu8_TrkIsoVVL_Ele23_CaloIdL_TrackIdL_IsoVL_DZ_v* |
| HLT_Ele23_Ele12_CaloIdL_TrackIdL_IsoVL_DZ_v* |
| HLT_Mu17_TrkIsoVVL_Mu8_TrkIsoVVL_DZ_v* |
| HLT_Mu17_TrkIsoVVL_TkMu8_TrkIsoVVL_DZ_v* |
| HLT_IsoMu22_v* |
| HLT_IsoTkMu22_v* |
| HLT_IsoMu22_eta2p1_v* |
| HLT_IsoTkMu22_eta2p1_v* |
| HLT_IsoMu24_v* |
| HLT_IsoTkMu24_v* |
| HLT_Ele27_WPTight_Gsf_v* |
| HLT_Ele25_eta2p1_WPTight_Gsf_v* |
| HLT_Ele27_eta2p1_WPLoose_Gsf_v* |

Table 4.5: Table of high-level triggers that we consider in the analysis.

997 4.2.2 Triggers

998 We consider online-reconstructed events triggered by one, two, or three leptons.
 999 Single-lepton triggers are included to boost the acceptance of events where the p_T of
 1000 the sub-leading lepton falls below the threshold of the double-lepton triggers. Ad-
 1001 ditionally, by including double-lepton triggers in the ≥ 3 lepton category, as well
 1002 as single-lepton triggers in all categories, we increase the efficiency, considering the
 1003 logical “or” of the trigger decisions of all the individual triggers in a given category.
 1004 Tab. 4.5 shows the lowest-threshold non-prescaled triggers present in the High-Level
 1005 Trigger (HLT) menus for both Monte-Carlo and data in 2016.

1006 4.2.2.1 Trigger efficiency scale factors

1007 The efficiency of events to pass the trigger is measured in simulation (trivially using
 1008 generator information) and in the data (using event collected by an uncorrelated

| Category | Scale Factor |
|----------|-----------------|
| ee | 1.01 ± 0.02 |
| e μ | 1.01 ± 0.01 |
| $\mu\mu$ | 1.00 ± 0.01 |
| 3l | 1.00 ± 0.03 |

Table 4.6: Trigger efficiency scale factors and associated uncertainties, shown here rounded to the nearest percent.

MET trigger). Small differences between the data and MC efficiencies are corrected by applying scale factors as shown in Tab. 4.6. The exact procedure and control plots are documented in [66] for the current analysis.

4.3 Object Identification and event selection

4.3.1 Jets and b tagging

The analysis uses anti- k_t (0.4) particle-flow (PF) jets, corrected for charged hadrons not coming from the primary vertex (charged hadron subtraction), and having jet energy corrections (`Summer16_23Sep2016V3`) applied as a function of the jet E_T and η . Jets are only considered if they have a transverse energy above 25GeV.

In addition, they are required to be separated from any lepton candidates passing the fakeable object selections (see Tables 4.7 and 4.8) by $\Delta R > 0.4$.

The loose and medium working points of the CSV b-tagging algorithm are used to identify b jets. Data/simulation differences in the b tagging performance are corrected by applying per-jet weights to the simulation, dependent on the jet p_T , eta, b tagging discriminator, and flavor (from simulation truth) [67]. The per-event weight is taken as the product of the per-jet weights, including those of the jets associated to the leptons. More details can be found in the corresponding $t\bar{t}H$ documentation [63, 66].

1026 **4.3.2 Lepton selection**

| Cut | Loose | Fakeable object | Tight |
|--------------------------------|-----------------|------------------|------------------|
| $ \eta < 2.4$ | ✓ | ✓ | ✓ |
| p_T | $> 5\text{GeV}$ | $> 15\text{GeV}$ | $> 15\text{GeV}$ |
| $ d_{xy} < 0.05 \text{ (cm)}$ | ✓ | ✓ | ✓ |
| $ d_z < 0.1 \text{ (cm)}$ | ✓ | ✓ | ✓ |
| $\text{SIP}_{3D} < 8$ | ✓ | ✓ | ✓ |
| $I_{\text{mini}} < 0.4$ | ✓ | ✓ | ✓ |
| is Loose Muon | ✓ | ✓ | ✓ |
| jet CSV | — | < 0.8484 | < 0.8484 |
| is Medium Muon | — | — | ✓ |
| tight-charge | — | — | ✓ |
| lepMVA > 0.90 | — | — | ✓ |

Table 4.7: Requirements on each of the three muon selections. In the cases where the cut values change between the selections, those values are listed in the table. Otherwise, whether the cut is applied is indicated. For the two p_T^{ratio} and CSV rows, the cuts marked with a † are applied to leptons that fail the lepton MVA cut, while the loose cut value is applied to those that pass the lepton MVA cut.

1027 The lepton reconstruction and selection is identical to that used in the $t\bar{t}H$ mul-
 1028 tilepton analysis, as documented in Refs. [63, 66]. For details on the reconstruction
 1029 algorithms, isolation, pileup mitigation, and a description of the lepton MVA discrim-
 1030 inator and validation plots thereof, we refer to that document since they are out of
 1031 the scope of this thesis. Three different selections are defined both for the electron
 1032 and muon object identification: the *Loose*, *Fakeable Object*, and *Tight* selection. As
 1033 described in more detail later, these are used for event level vetoes, the fake rate
 1034 estimation application region, and the final signal selection, respectively. The p_T of
 1035 fakeable objects is defined as $0.85 \times p_T(\text{jet})$, where the jet is the one associated to the
 1036 lepton object. This mitigates the dependence of the fake rate on the momentum of
 1037 the fakeable object and thereby improves the precision of the method.

1038 Tables 4.7 and 4.8 list the full criteria for the different selections of muons and
 1039 electrons.

| Cut | Loose | Fakeable Object | Tight |
|--|-----------------|----------------------------|------------------|
| $ \eta < 2.5$ | ✓ | ✓ | ✓ |
| p_T | $> 7\text{GeV}$ | $> 15\text{GeV}$ | $> 15\text{GeV}$ |
| $ d_{xy} < 0.05 \text{ (cm)}$ | ✓ | ✓ | ✓ |
| $ d_z < 0.1 \text{ (cm)}$ | ✓ | ✓ | ✓ |
| $\text{SIP}_{3D} < 8$ | ✓ | ✓ | ✓ |
| $I_{\text{mini}} < 0.4$ | ✓ | ✓ | ✓ |
| MVA ID $> (0.0, 0.0, 0.7)$ | ✓ | ✓ | ✓ |
| $\sigma_{i\eta i\eta} < (0.011, 0.011, 0.030)$ | — | ✓ | ✓ |
| $\text{H/E} < (0.10, 0.10, 0.07)$ | — | ✓ | ✓ |
| $\Delta\eta_{in} < (0.01, 0.01, 0.008)$ | — | ✓ | ✓ |
| $\Delta\phi_{in} < (0.04, 0.04, 0.07)$ | — | ✓ | ✓ |
| $-0.05 < 1/E - 1/p < (0.010, 0.010, 0.005)$ | — | ✓ | ✓ |
| p_T^{ratio} | — | $> 0.5 \dagger / -$ | — |
| jet CSV | — | $< 0.3 \dagger / < 0.8484$ | < 0.8484 |
| tight-charge | — | — | ✓ |
| conversion rejection | — | — | ✓ |
| Number of missing hits | < 2 | $== 0$ | $== 0$ |
| lepMVA > 0.90 | — | — | ✓ |

Table 4.8: Criteria for each of the three electron selections. In cases where the cut values change between selections, those values are listed in the table. Otherwise, whether the cut is applied is indicated. In some cases, the cut values change for different η ranges. These ranges are $0 < |\eta| < 0.8$, $0.8 < |\eta| < 1.479$, and $1.479 < |\eta| < 2.5$ and the respective cut values are given in the form (value₁, value₂, value₃).

1040 4.3.3 Lepton selection efficiency

1041 Efficiencies of reconstruction and selecting loose leptons are measured both for muons
 1042 and electrons using a tag and probe method on both data and MC, using $Z \rightarrow \ell^+\ell^-$.
 1043 Corresponding scale factors are derived from the ratio of efficiencies and applied to the
 1044 selected These. Events are produced for the leptonic SUSY analyses using equivalent
 1045 lepton selections and recycled for the $t\bar{t}H$ analysis as well as for this analysis. The
 1046 efficiencies of applying the tight selection as defined in Tables 4.7 and 4.8, on the
 1047 loose leptons are determined again by using a tag and probe method on a sample of
 1048 DY-enriched events. They are documented for the $t\bar{t}H$ analysis in Ref. [66] and are
 1049 exactly equivalent for this analysis.

1050 4.4 Background predictions

1051 The modeling of reducible and irreducible backgrounds in this analysis uses the exact
 1052 methods, analysis code, and ROOT trees used for the $t\bar{t}H$ multilepton analysis. We
 1053 give a brief description of the methods and refer to the documentation of that analysis
 1054 in Refs. [63, 66] for any details.

1055 The backgrounds in three-lepton final states can be split in two broad categories:
 1056 irreducible backgrounds with genuine prompt leptons (i.e. from on-shell W and Z
 1057 boson decays); and reducible backgrounds where at least one of the leptons is “non-
 1058 prompt”, i.e. produced within a hadronic jet, either a genuine lepton from heavy
 1059 flavor decays, or simply mis-reconstructed jets.

1060 Irreducible backgrounds can be reliably estimated directly from Monte-Carlo sim-
 1061 ulated events, using higher-order cross sections or data control regions for the overall
 1062 normalization. This is done in this analysis for all backgrounds involving prompt lep-
 1063 tons: $t\bar{t}W$, $t\bar{t}Z$, $t\bar{t}H$, WZ , ZZ , $W^\pm W^\pm qq$, $t\bar{t}t\bar{t}$, tZq , tZW , WWW , WWZ , WZZ ,
 1064 ZZZ .

1065 Reducible backgrounds, on the other hand, are not well predicted by simulation,
 1066 and are estimated using data-driven methods. In the case of non-prompt leptons, a
 1067 fake rate method is used, where the contribution to the final selection is estimated by
 1068 extrapolating from a sideband (or “application region”) with a looser lepton definition
 1069 (the fakeable object definitions in Tabs. 4.7 and 4.8) to the signal selection. The tight-
 1070 to-loose ratios (or “fake rates”) are measured in several background dominated data
 1071 events with dedicated triggers, subtracting the residual prompt lepton contribution
 1072 using MC. Non-prompt leptons in our signal regions are predominantly produced in $t\bar{t}$
 1073 events, with a much smaller contribution, from Drell–Yan production. The systematic
 1074 uncertainty on the normalization of the non-prompt background estimation is on the

order of 50%, and thereby one of the dominant limitations on the performance of multilepton analyses in general and this analysis in particular. It consists of several individual sources, such as the result of closure tests of the method using simulated events, limited statistics in the data control regions due to necessary prescaling of lepton triggers, and the uncertainty in the subtraction of residual prompt leptons from the control region.

The fake background where the leptons pass the looser selection are weighted according to how many of them fail the tight criteria. Events with a single failing lepton are weighted with the factor $f/(1-f)$ for the estimate to the tight selection region, where f is the fake rate. Events with two failing leptons are given the negative weight $-f_i f_j / (1-f_i)(1-f_j)$, and for three leptons the weight is positive and equal to the product of $f/(1-f)$ factor evaluated for each failing lepton.

Figures 4.2 show the distributions of some relevant kinematic variables, normalized to the cross section of the respective processes and to the integrated luminosity.

4.5 Signal discrimination

The tHq signal is separated from the main backgrounds using a boosted decision tree (BDT) classifier, trained on simulated signal and background events. A set of discriminating variables are given as input to the BDT which produces a output distribution maximizing the discrimination power. Table 4.9 lists the input variables used while Figures 4.3 show their distributions for the relevant signal and background samples, for the three lepton channel. Two BDT classifiers are trained for the two main backgrounds expected in the analysis: events with prompt leptons from $t\bar{t}W$ and $t\bar{t}Z$ (also referred to as $t\bar{t}V$), and events with non-prompt leptons from $t\bar{t}$. The datasets used in the training are the tHq signal (see Tab. 4.1), and LO MADGRAPH samples

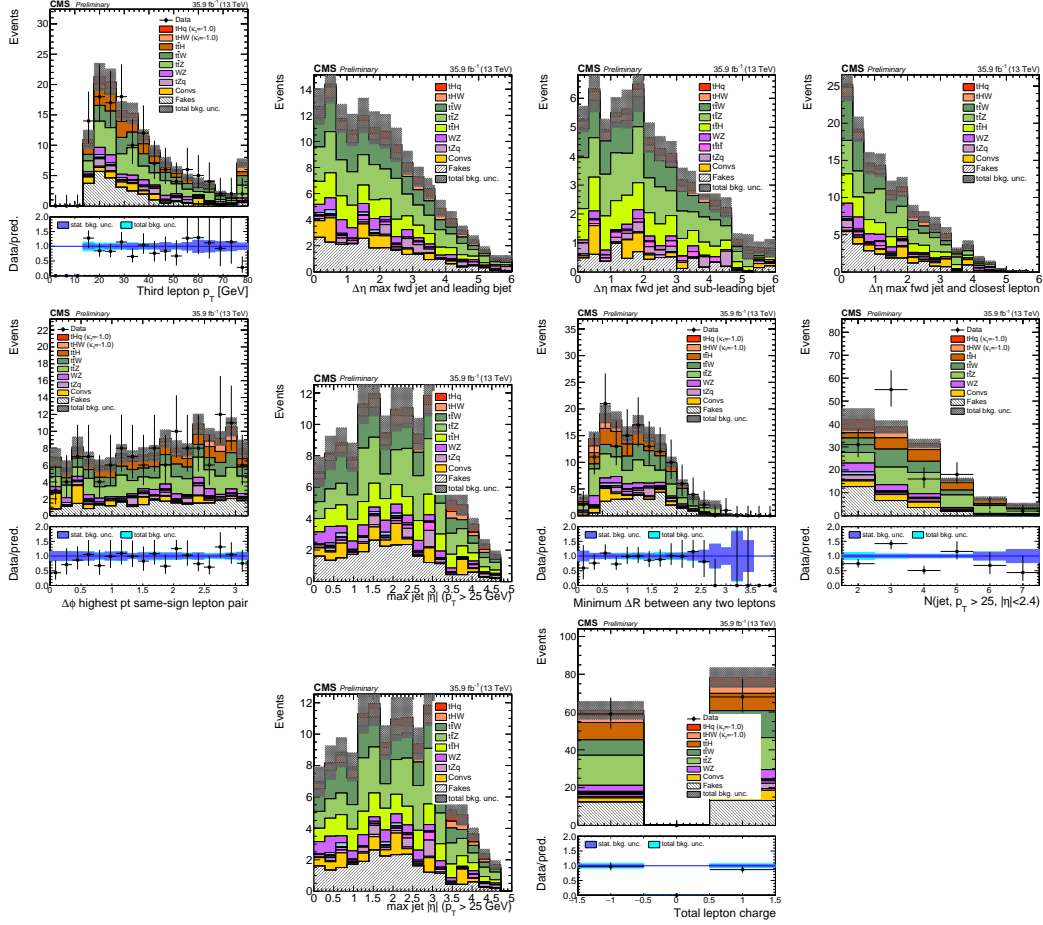


Figure 4.2: Distributions of input variables to the BDT for signal discrimination, three lepton channel, normalized to their cross section and to 35.9fb^{-1} .

of $t\bar{t}W$ and $t\bar{t}Z$, in an admixture proportional to their respective cross sections (see Tab. 4.4).

The MVA analysis consist of two stages: first a “training” where the MVA method is trained to discriminate between simulated signal and background events, then a “test” stage where the trained algorithm is used to classify different events from the samples. The sample is obtained from a pre-selection (see Tab. ?? with pre-selection cuts). Figures 4.4 show the input variables distributions as seen by the MVA algorithm. Note that in contrast to the distributions in Fig. 4.3 only the main backgrounds ($t\bar{t}$ from simulation, $t\bar{t}V$) are included.

| Variable name | Description |
|----------------------|--|
| nJet25 | Number of jets with $p_T > 25$ GeV, $ \eta < 2.4$ |
| MaxEtaJet25 | Maximum $ \eta $ of any (non-CSV-loose) jet with $p_T > 25$ GeV |
| totCharge | Sum of lepton charges |
| nJetEta1 | Number of jets with $ \eta > 1.0$, non-CSV-loose |
| detaFwdJetBJet | $\Delta\eta$ between forward light jet and hardest CSV loose jet |
| detaFwdJet2BJet | $\Delta\eta$ between forward light jet and second hardest CSV loose jet (defaults to -1 in events with only one CSV loose jet) |
| detaFwdJetClosestLep | $\Delta\eta$ between forward light jet and closest lepton |
| dphiHighestPtSSPair | $\Delta\phi$ of highest p_T same-sign lepton pair |
| minDRll | minimum ΔR between any two leptons |
| Lep3Pt/Lep2Pt | p_T of the 3 rd lepton (2 nd for ss2l) |

Table 4.9: MVA input discriminating variables

1108 Note that splitting the training in two groups reveals that some variables show
 1109 opposite behavior for the two background sources; potentially screening the discrimi-
 1110 nation power if they were to be used in a single discriminant. For some other variables
 1111 the distributions are similar in both background cases.

1112 From table 4.9, it is clear that the input variables are correlated to some extend.
 1113 These correlations play an important role for some MVA methods like the Fisher
 1114 discriminant method in which the first step consist of performing a linear transfor-
 1115 mation to an phase space where the correlations between variables are removed. In
 1116 case a boosted decision tree (BDT) method however, correlations do not affect the
 1117 performance. Figure 4.6 show the linear correlation coefficients for signal and back-
 1118 ground for the two training cases (the signal values are identical by construction). As
 1119 expected, strong correlations appears for variables related to the forward jet activity.
 1120 Same trend is seen in case of the same sign dilepton channel in Figure ??.

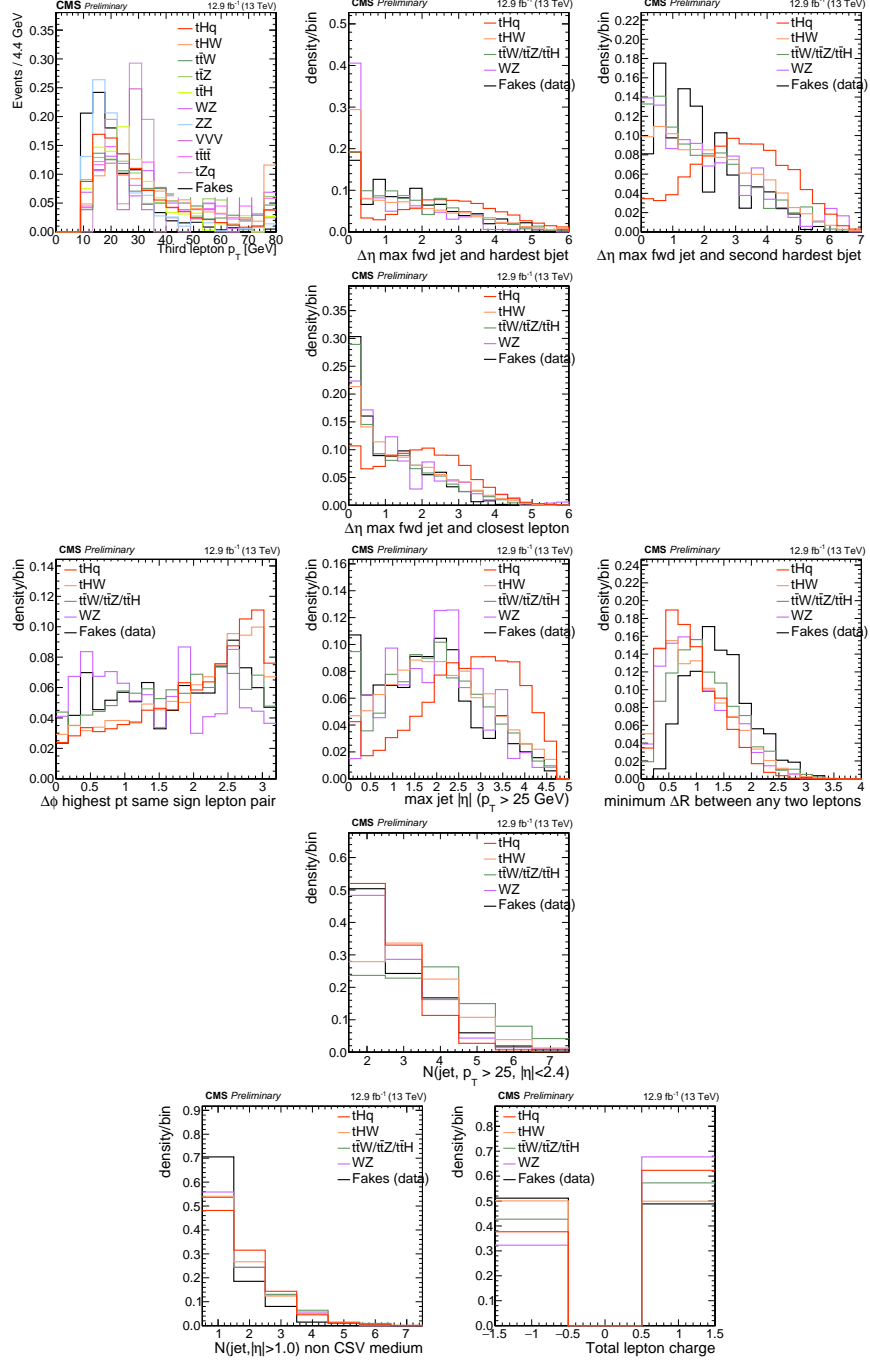


Figure 4.3: Distributions of input variables to the BDT for signal discrimination, three lepton channel.

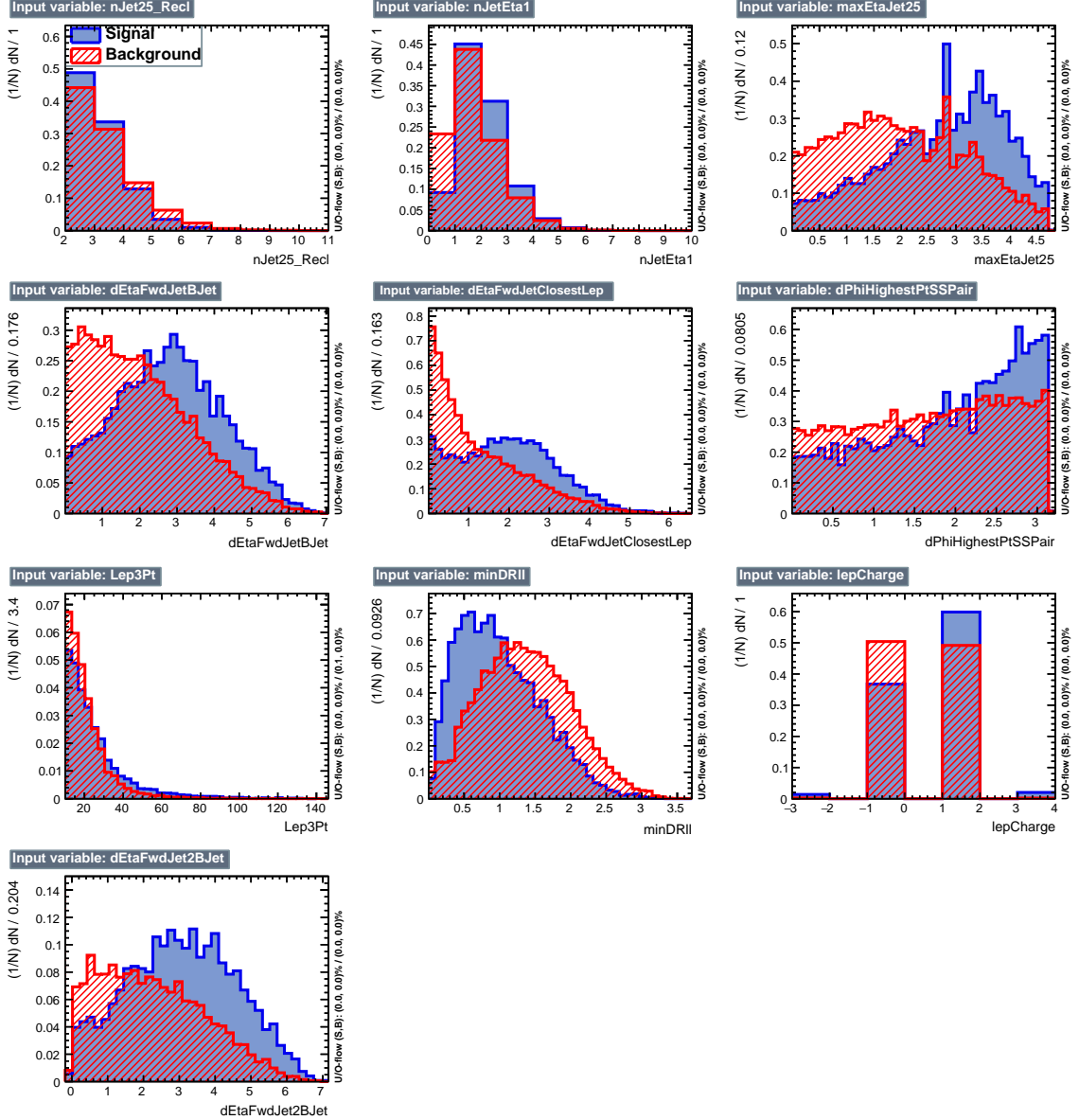


Figure 4.4: BDT inputs as seen by TMVA (signal, in blue, is tHq , background, in red, is $t\bar{t}$) for the three lepton channel, discriminated against $t\bar{t}$ (fakes) background.

1121 4.5.1 Classifiers response

1122 Several MVA algorithms were evaluated to determine the most appropriate method
 1123 for this analysis. The plots in Fig. 4.7 (top) show the background rejection as a
 1124 function of the signal efficiency for $t\bar{t}$ and $t\bar{t}V$ trainings (ROC curves) for the different

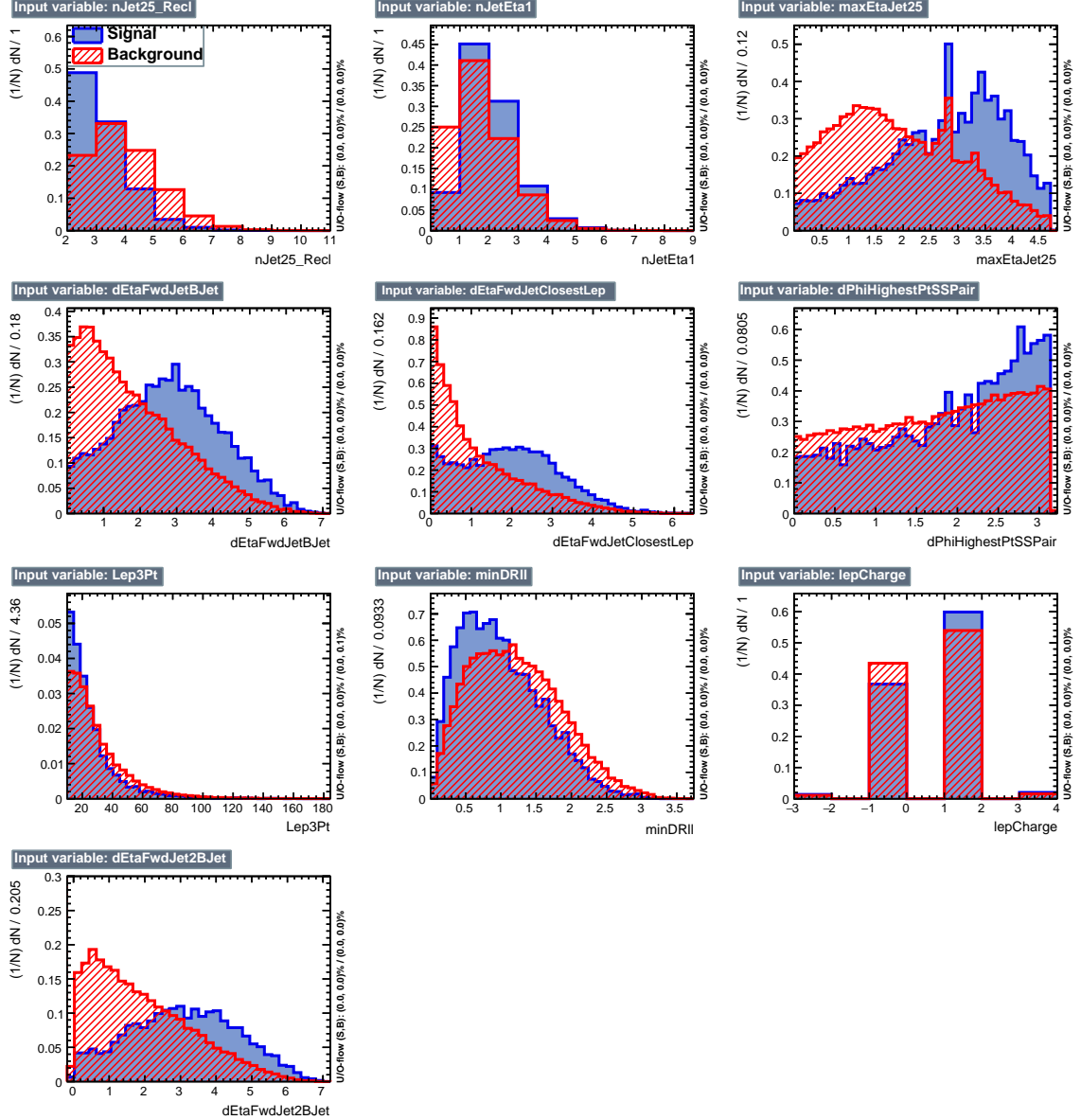


Figure 4.5: BDT inputs as seen by TMVA (signal, in blue, is tHq , background, in red, is $t\bar{t}W+t\bar{t}Z$) for the three lepton channel, discriminated against $t\bar{t}V$ background.

algorithms that were evaluated.

In both cases the gradient boosted decision tree (“BDTA_GRAD”) classifier offers the best results, followed by an adaptive BDT classifier (“BDTA”). The BDTA_GRAD classifier output distributions for signal and backgrounds are shown on the bottom of Fig. 4.7. As expected, a good discrimination power is obtained using default discrim-

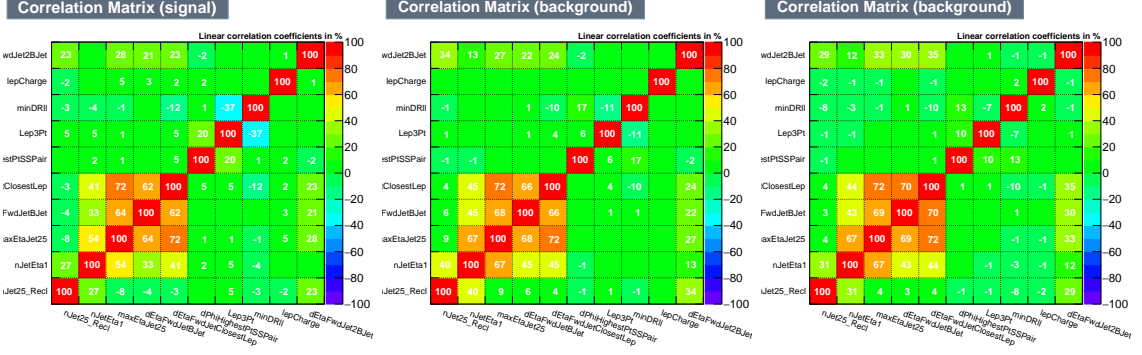


Figure 4.6: Signal (left), $t\bar{t}$ background (middle), and $t\bar{t}V$ background (right.) correlation matrices for the input variables in the TMVA analysis for the three lepton channel.

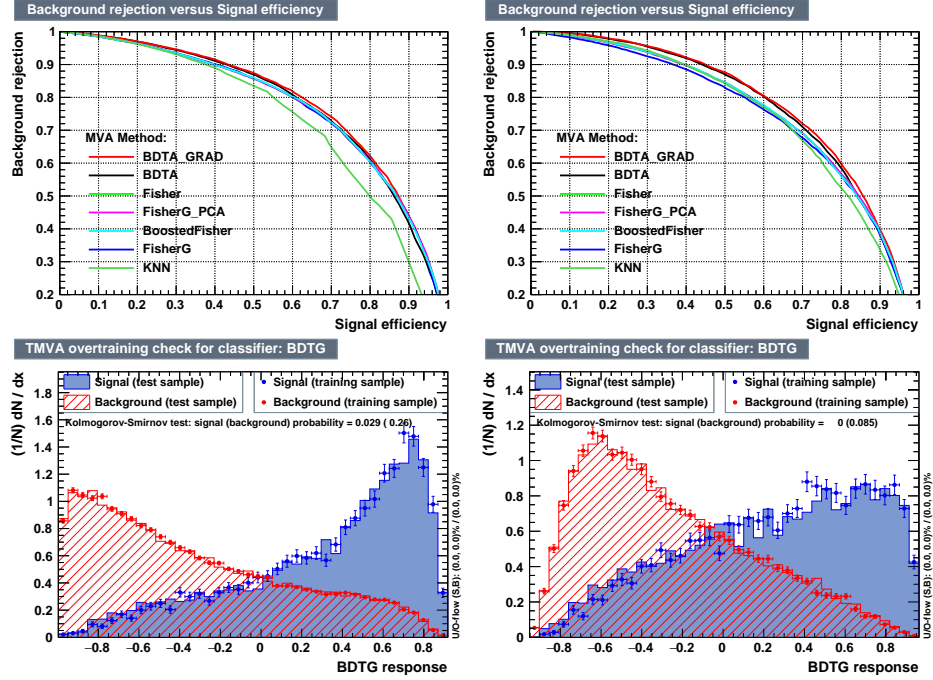


Figure 4.7: Top: background rejection vs signal efficiency (ROC curves) for various MVA classifiers (top) in the three lepton channel against $t\bar{t}V$ (left) and $t\bar{t}$ (right). Bottom: classifier output distributions for the gradient boosted decision trees, for training against $t\bar{t}V$ (left) and against $t\bar{t}$ (right).

1130 inator parameter values, with minimal overtraining. TMVA provides a ranking of the
 1131 input variables by their importance in the classification process, shown in Tab. 4.10.
 1132 The TMVA settings used in the BDT training are shown in Tab. 4.11.

| ttbar training | | | ttV training | | |
|----------------|----------------------|------------|----------------------|------------|--|
| Rank | Variable | Importance | Variable | Importance | |
| 1 | minDRll | 1.329e-01 | dEtaFwdJetBJet | 1.264e-01 | |
| 2 | dEtaFwdJetClosestLep | 1.294e-01 | Lep3Pt | 1.224e-01 | |
| 3 | dEtaFwdJetBJet | 1.209e-01 | maxEtaJet25 | 1.221e-01 | |
| 4 | dPhiHighestPtSSPair | 1.192e-01 | dEtaFwdJet2BJet | 1.204e-01 | |
| 5 | Lep3Pt | 1.158e-01 | dEtaFwdJetClosestLep | 1.177e-01 | |
| 6 | maxEtaJet25 | 1.121e-01 | minDRll | 1.143e-01 | |
| 7 | dEtaFwdJet2BJet | 9.363e-02 | dPhiHighestPtSSPair | 9.777e-02 | |
| 8 | nJetEta1 | 6.730e-02 | nJet25_Recl | 9.034e-02 | |
| 9 | nJet25_Recl | 6.178e-02 | nJetEta1 | 4.749e-02 | |
| 10 | lepCharge | 4.701e-02 | lepCharge | 4.116e-02 | |

Table 4.10: TMVA input variables ranking for BDTA_GRAD method for the trainings in the three lepton channel. For both trainings the rankings show almost the same 5 variables in the first places.

```
TMVA.Types.kBDT
NTrees=800
BoostType=Grad
Shrinkage=0.10
!UseBaggedGrad
nCuts=50
MaxDepth=3
NegWeightTreatment=PairNegWeightsGlobal
CreateMVApdfs
```

Table 4.11: TMVA configuration used in the BDT training.

1133 4.6 Additional discriminating variables

1134 Two additional discriminating variables were tested considering the fact that the
 1135 forward jet in the background could come from the pileup; since we have a real
 1136 forward jet in the signal, it could give some improvement in the discriminating power.
 1137 The additional variables describe the forward jet momentum (fwdJetPt25) and the
 1138 forward jet identification(fwdJetPUID). Distributions for these variables in the three
 1139 lepton channel are shown in the figure 4.8. The forward jet identification distribution
 1140 show that for both, signal and background, jets are mostly real jets.

1141 The testing was made including in the MVA input one variable at a time, so we

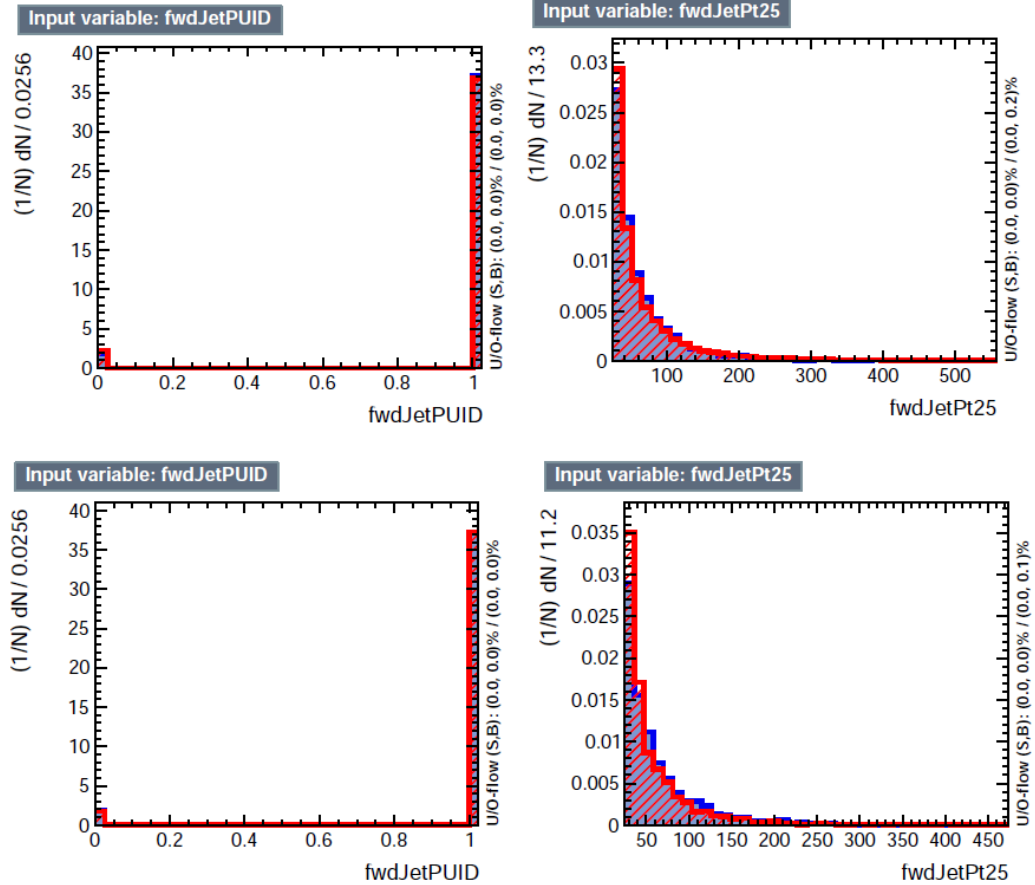


Figure 4.8: Additional discriminating variables distributions for ttV training (Top row) and tt training (bottom row) in the three lepton channel. The origin of the jets in the forward jet identification distribution is tagged as 0 for “pileup jets” while “real jets” are tagged as 1.

1142 can evaluate the discrimination power of each variable, and then both simultaneously.
 1143 fwdJetPUID was ranked in the last place in importance (11) in both training (ttV
 1144 and tt) while fwdJetPt25 was ranked 3 in the ttV training and 7 in the tt training.
 1145 When training using 12 variables, fwdJetPt25 was ranked 5 and 7 in the ttV and tt
 1146 trainings respectively, while fwdJetPUID was ranked 12 in both cases.

1147 The improvement in the discrimination performance provided by the additional
 1148 variables is about 1%, so it was decided not to include them in the procedure. Table
 1149 4.12 show the ROC-integral for all the testing cases we made.

| ROC-integral | |
|------------------|-------|
| base 10 var ttv | 0.848 |
| + fwdJetPUID ttv | 0.849 |
| + fwdJetPt25 ttv | 0.856 |
| 12 var ttv | 0.856 |
| <hr/> | |
| base 10 var tt | 0.777 |
| + fwdJetPUID tt | 0.777 |
| + fwdJetPt25 tt | 0.787 |
| 12 var | 0.787 |

Table 4.12: ROC-integral for all the testing cases we made in the evaluation of the additional variables discriminating power. The improvement in the discrimination performance provided by the additional variables is about 1%

₁₁₅₀ **Chapter 5**

₁₁₅₁ **The CMS forward pixel detector**

₁₁₅₂ **5.0.1 The phase 1 FPix upgrade**

₁₁₅₃ **5.0.2 FPix module production line**

₁₁₅₄ **5.0.3 The Gluing stage**

₁₁₅₅ **5.0.4 The Encapsulation stage**

₁₁₅₆ **5.0.5 The FPix module production yields**

¹¹⁵⁷ References

- ¹¹⁵⁸ [1] D.J. Griffiths, “Introduction to electrodynamics”. 4th ed. Pearson, (2013).
- ¹¹⁵⁹ [2] F. Mandl, G. Shaw. “Quantum field theory.” Chichester: Wiley (2009).
- ¹¹⁶⁰ [3] F. Halzen, and A.D. Martin, “Quarks and leptons: An introductory course in
¹¹⁶¹ modern particle physics”. New York: Wiley, (1984) .
- ¹¹⁶² [4] J.C. Maxwell. “A dynamical theory of the electromagnetic field”. Philosophical Transactions of the Royal Society of London. 155: 459–512.(1865)
¹¹⁶³
¹¹⁶⁴ doi:10.1098/rstl.1865.0008
- ¹¹⁶⁵ [5] M. Planck. “Über das Gesetz der Energieverteilung im Normalspektrum”.
¹¹⁶⁶ Annalen der Physik. 4 (3): 553.(1901).
- ¹¹⁶⁷ [6] A. Einstein “Über einen die Erzeugung und Verwandlung des Lichtes betref-
¹¹⁶⁸ fenden heuristischen Gesichtspunkt”. Annalen der Physik. 17 (6): 132–148,
¹¹⁶⁹ (1905).
- ¹¹⁷⁰ [7] A. Einstein. “Über die von der molekularkinetischen Theorie der Wärme
¹¹⁷¹ geforderte Bewegung von in ruhenden Flüssigkeiten suspendierten Teilchen”.
¹¹⁷² Annalen der Physik. 17 (8): 549–560, (1905).
- ¹¹⁷³ [8] A. Einstein. “Zur Elektrodynamik bewegter Körper”. Annalen der Physik. 17
¹¹⁷⁴ (10): 891–921, (1905).

- 1175 [9] A. Einstein, "Ist die TrÄdgheit eines KÃürpers von seinem Energieinhalt ab-
 1176 hÃdngig?". Annalen der Physik. 18 (13): 639â€¢641, (1905).
- 1177 [10] B. P. Abbott et al. "Observation of Gravitational Waves from a Binary Black
 1178 Hole Merger". PRL 116, 061102 (2016).
- 1179 [11] J. Schwinger. "Quantum Electrodynamics. I. A Covariant Formulation". Phys-
 1180 ical Review. 74 (10): 1439â€¢61, (1948).
- 1181 [12] R. P. Feynman. "Spaceâ€¢Time Approach to Quantum Electrodynamics".
 1182 Physical Review. 76 (6): 769â€¢89, (1949).
- 1183 [13] S. Tomonaga. "On a Relativistically Invariant Formulation of the Quantum
 1184 Theory of Wave Fields". Progress of Theoretical Physics. 1 (2): 27â€¢42, (1946).
- 1185 [14] S.L. Glashow. "Partial symmetries of weak interactions", Nucl. Phys. 22 579-
 1186 588, (1961).
- 1187 [15] A. Salam, J.C. Ward. "Electromagnetic and weak interactions", Physics Letters
 1188 13 168-171, (1964).
- 1189 [16] S. Weinberg, "A model of leptons", Physical Review Letters, vol. 19, no. 21, p.
 1190 1264, (1967).
- 1191 [17] E. Noether, "Invariante Variationsprobleme", Nachrichten von der Gesellschaft
 1192 der Wissenschaften zu GÃüttingen, mathematisch-physikalische Klasse, vol.
 1193 1918, pp. 235â€¢257, (1918).
- 1194 [18] File:Standard_Model_of_Elementary_Particle_dark.svg. (2017, June 12)
 1195 Wikimedia Commons, the free media repository. Retrieved November 27,
 1196 2017 from <https://www.collegiate-advanced-electricity.com/single-post/2017/04/10/The-Standard-Model-of-Particle-Physics>.

- 1198 [19] M. Goldhaber, L. Grodzins, A.W. Sunyar “Helicity of Neutrinos”, Phys. Rev.
 1199 109, 1015 (1958).
- 1200 [20] Palanque-Delabrouille N et al. “Neutrino masses and cosmology with Lyman-
 1201 alpha forest power spectrum”, JCAP 11 011 (2015).
- 1202 [21] C. Patrignani et al. (Particle Data Group), Chin. Phys. C, 40, 100001 (2016)
 1203 and 2017 update.
- 1204 [22] M. Gell-Mann. “A Schematic Model of Baryons and Mesons”. Physics Letters.
 1205 8 (3): 214–215 (1964).
- 1206 [23] G. Zweig. “An SU(3) Model for Strong Interaction Symmetry and its Breaking”
 1207 (PDF). CERN Report No.8182/TH.401 (1964).
- 1208 [24] G. Zweig. “An SU(3) Model for Strong Interaction Symmetry and its Breaking:
 1209 II” (PDF). CERN Report No.8419/TH.412(1964).
- 1210 [25] M. Gell-Mann. “The Interpretation of the New Particles as Displaced Charged
 1211 Multiplets”. Il Nuovo Cimento 4: 848. (1956).
- 1212 [26] T. Nakano, K. Nishijima. “Charge Independence for V-particles”. Progress of
 1213 Theoretical Physics 10 (5): 581-582. (1953).
- 1214 [27] N. Cabibbo, “Unitary symmetry and leptonic decays” Physical Review Letters,
 1215 vol. 10, no. 12, p. 531, (1963).
- 1216 [28] M.Kobayashi, T.Maskawa, “CP-violation in the renormalizable theory of weak
 1217 interaction,” Progress of Theoretical Physics, vol. 49, no. 2, pp. 652-657, (1973).
- 1218 [29] File:Weak Decay (flipped).svg. (2017, June 12). Wikimedia Com-
 1219 mons, the free media repository. Retrieved November 27, 2017

- 1220 from `https : //commons.wikimedia.org/w/index.php?title = File :`
 1221 `Weak_Decay_(flipped).svg&oldid = 247498592.`
- 1222 [30] Georgia Tech University. Coupling Constants for the Fundamental
 1223 Forces(2005). Retrieved January 10, 2018, from `http://hyperphysics.phy –`
 1224 `astr.gsu.edu/hbase/Forces/couple.html#c2`
- 1225 [31] M. Strassler. (May 31, 2013).The Strengths of the Known Forces. Retrieved
 1226 January 10, 2018, from `https://profmattstrassler.com/articles – and –`
 1227 `posts/particle – physics – basics/the – known – forces – of – nature/the –`
 1228 `strength – of – the – known – forces/`
- 1229 [32] M. Peskin, D. Schroeder, “An introduction to quantum field theory”. Perseus
 1230 Books Publishing L.L.C., (1995).
- 1231 [33] A. Pich. “The Standard Model of Electroweak Interactions”
 1232 `https://arxiv.org/abs/1201.0537`
- 1233 [34] F.Bellaiche. (2012, 2 September). “What’s this Higgs boson anyway?”. Retrieved
 1234 from: `https://www.quantum-bits.org/?p=233`
- 1235 [35] M. Endres et al. Nature 487, 454-458 (2012) doi:10.1038/nature11255
- 1236 [36] F. Englert, R. Brout. “Broken Symmetry and the Mass of Gauge Vec-
 1237 tor Mesons”. Physical Review Letters. 13 (9): 321–323.(1964) Bib-
 1238 code:1964PhRvL..13..321E. doi:10.1103/PhysRevLett.13.321
- 1239 [37] P.Higgs. “Broken Symmetries and the Masses of Gauge Bosons”. Physical
 1240 Review Letters. 13 (16): 508–509,(1964). Bibcode:1964PhRvL..13..508H.
 1241 doi:10.1103/PhysRevLett.13.508.

- 1242 [38] G.Guralnik, C.R. Hagen and T.W.B. Kibble. “Global Conservation Laws and
 1243 Massless Particles”. Physical Review Letters. 13 (20): 585–587, (1964). Bib-
 1244 code:1964PhRvL..13..585G. doi:10.1103/PhysRevLett.13.585.
- 1245 [39] CMS collaboration. “Observation of a new boson at a mass of 125
 1246 GeV with the CMS experiment at the LHC”. Physics Letters B.
 1247 716 (1): 30–61 (2012). arXiv:1207.7235. Bibcode:2012PhLB..716...30C.
 1248 doi:10.1016/j.physletb.2012.08.021
- 1249 [40] ATLAS collaboration. “Observation of a New Particle in the Search for the Stan-
 1250 dard Model Higgs Boson with the ATLAS Detector at the LHC”. Physics Let-
 1251 ters B. 716 (1): 1–29(2012). arXiv:1207.7214 Bibcode:2012PhLB..716....1A.
 1252 doi:10.1016/j.physletb.2012.08.020.
- 1253 [41] ATLAS collaboration; CMS collaboration (26 March 2015). “Combined
 1254 Measurement of the Higgs Boson Mass in pp Collisions at $\sqrt{s}=7$ and
 1255 8 TeV with the ATLAS and CMS Experiments”. Physical Review Let-
 1256 ters. 114 (19): 191803. arXiv:1503.07589. Bibcode:2015PhRvL.114s1803A.
 1257 doi:10.1103/PhysRevLett.114.191803.
- 1258 [42] CMS Collaboration, “SM Higgs Branching Ratios and To-
 1259 tal Decay Widths (up-date in CERN Report4 2016)”.
 1260 <https://twiki.cern.ch/twiki/bin/view/LHCPhysics/CERNYellowReportPageBR>
 1261 , last accessed on 17.12.2017.
- 1262 [43] R.Grant V. “Determination of Higgs branching ratios in $H \rightarrow W^+W^- \rightarrow l^+l^- jj$ and $H \rightarrow ZZ \rightarrow l^+l^- jj$ channels”. Physics Department, Uni-
 1263 versity of Tennessee (Dated: October 31, 2012). Retrieved from
 1264 <http://aesop.phys.utk.edu/ph611/2012/projects/Riley.pdf>

- 1266 [44] LHC Higgs Cross Section Working Group, Denner, A., Heinemeyer, S. et al.
 1267 “Standard model Higgs-boson branching ratios with uncertainties”. Eur. Phys.
 1268 J. C (2011) 71: 1753. <https://doi.org/10.1140/epjc/s10052-011-1753-8>
- 1269 [45] LHC InternationalMasterclasses“When protons collide”. Retrieved from
 1270 http://atlas.physicsmasterclasses.org/en/zpath_protoncollisions.htm
- 1271 [46] F. Maltoni, K. Paul, T. Stelzer, and S. Willenbrock, “Associated production
 1272 of Higgs and single top at hadron colliders”, Phys.Rev. D64 (2001) 094023,
 1273 [hep-ph/0106293].
- 1274 [47] S. Biswas, E. Gabrielli, F. Margaroli, and B. Mele, “Direct constraints on the
 1275 top-Higgs coupling from the 8 TeV LHC data,” Journal of High Energy Physics,
 1276 vol. 07, p. 073, (2013).
- 1277 [48] M. Farina, C. Grojean, F. Maltoni, E. Salvioni, and A. Thamm, “Lifting de-
 1278 generacies in Higgs couplings using single top production in association with a
 1279 Higgs boson,” Journal of High Energy Physics, vol. 05, p. 022, (2013).
- 1280 [49] T.M. Tait and C.-P. Yuan, “Single top quark production as a window to physics
 1281 beyond the standard model”, Phys. Rev. D 63 (2000) 014018 [hep-ph/0007298].
- 1282 [50] F. Demartin, F. Maltoni, K. Mawatari, and M. Zaro, “Higgs production in
 1283 association with a single top quark at the LHC,” European Physical Journal C,
 1284 vol. 75, p. 267, (2015).
- 1285 [51] CMS Collaboration, “Modelling of the single top-quark pro-
 1286 duction in association with the Higgs boson at 13 TeV.”
 1287 <https://twiki.cern.ch/twiki/bin/viewauth/CMS/SingleTopHiggsGeneration13TeV>,
 1288 last accessed on 16.01.2018.

- 1289 [52] CMS Collaboration, “SM Higgs production cross sections at $\sqrt{s} = 13$ TeV.”
1290 <https://twiki.cern.ch/twiki/bin/view/LHCPhysics/CERNYellowReportPageAt13TeV>,
1291 last accessed on 16.01.2018.
- 1292 [53] S. Dawson, The effective W approximation, Nucl. Phys. B 249 (1985) 42.
- 1293 [54] S. Biswas, E. Gabrielli and B. Mele, JHEP 1301 (2013) 088 [arXiv:1211.0499
1294 [hep-ph]].
- 1295 [55] F. Demartin, B. Maier, F. Maltoni, K. Mawatari, and M. Zaro, “tWH associated
1296 production at the LHC”, European Physical Journal C, vol. 77, p. 34, (2017).
1297 arXiv:1607.05862
- 1298 [56] LHC Higgs Cross Section Working Group, “Handbook of LHC Higgs Cross
1299 Sections: 4.Deciphering the Nature of the Higgs Sector”, arXiv:1610.07922.
- 1300 [57] J. Ellis, D. S. Hwang, K. Sakurai, and M. Takeuchi.“Disentangling Higgs-Top
1301 Couplings in Associated Production”, JHEP 1404 (2014) 004, [arXiv:1312.5736].
- 1302 [58] CMS Collaboration, V. Khachatryan et al., “Precise determination of the mass
1303 of the Higgs boson and tests of compatibility of its couplings with the standard
1304 model predictions using proton collisions at 7 and 8 TeV,” arXiv:1412.8662.
- 1305 [59] ATLAS Collaboration, G. Aad et al., “Updated coupling measurements of the
1306 Higgs boson with the ATLAS detector using up to 25 fb^{-1} of proton-proton
1307 collision data”, ATLAS-CONF-2014-009.
- 1308 [60] ATLAS and CMS Collaborations, “Measurements of the Higgs boson produc-
1309 tion and decay rates and constraints on its couplings from a combined ATLAS
1310 and CMS analysis of the LHC pp collision data at $\sqrt{s} = 7$ and 8 TeV,” (2016).
1311 CERN-EP-2016-100, ATLAS-HIGG-2015-07, CMS-HIG-15-002.

- 1312 [61] CMS Collaboration, “Search for the associated production of a Higgs boson
 1313 with a single top quark in proton-proton collisions at $\sqrt{s} = 8$ TeV”, JHEP 06
 1314 (2016) 177,doi:10.1007/JHEP06(2016)177, arXiv:1509.08159.
- 1315 [62] B. Stieger, C. Jorda Lope et al., “Search for Associated Production of a Single
 1316 Top Quark and a Higgs Boson in Leptonic Channels”, CMS Analysis Note CMS
 1317 AN-14-140, 2014.
- 1318 [63] M. Peruzzi, C. Mueller, B. Stieger et al., “Search for ttH in multilepton final
 1319 states at $\sqrt{s} = 13$ TeV”, CMS Analysis Note CMS AN-16-211, 2016.
- 1320 [64] CMS Collaboration, “Search for H to bbar in association with a single top quark
 1321 as a test of Higgs boson couplings at $\sqrt{s} = 13$ TeV”, CMS Physics Analysis
 1322 Summary CMS-PAS-HIG-16-019, 2016.
- 1323 [65] B. Maier, “SingleTopHiggProduction13TeV”, February, 2016.
 1324 <https://twiki.cern.ch/twiki/bin/viewauth/CMS/SingleTopHiggsGeneration13TeV>.
- 1325 [66] M. Peruzzi, F. Romeo, B. Stieger et al., “Search for ttH in multilepton final1
 1326 states at $\sqrt{s} = 13$ TeV”, CMS Analysis Note CMS AN-17-029, 2017.
- 1327 [67] B. WG, “BtagRecommendation80XReReco”, February, 2017.
 1328 <https://twiki.cern.ch/twiki/bin/view/CMS/BtagRecommendation80XReReco>.